Received: 11 June 2019 | Revised: 21 October 2019 | Accepted: 30 October 2019

DOI: 10.1002/qua.26108

FULL PAPER

International Journal of QUANTUM CHEMISTRY WILEY

Insights into the role of D-A-π-A type pro-aromatic organic dyes with thieno[3,4-b]pyrazine as A acceptor group into dye-sensitized solar-cells. A TD-DFT/periodic DFT study

Katherine Paredes-Gil[1] | Dayán Páez-Hernández[2,3] | Ramiro Arratia-Pérez[2,3] | Fernando Mendizábal[3,4]

[1]Programa Institucional de Fomento a la Investigación, Desarrollo e Innovación, Universidad Tecnológica Metropolitana, Santiago, Chile

[2]Relativistic Molecular Physics (ReMoPh) Group, Facultad de Ciencias Exactas, Universidad Andres Bello, Santiago, Chile

[3]Núcleo Milenio de Ingeniería Molecular para Catálisis y Biosensores, ICM, Santiago, Chile

[4]Facultad de Ciencias, Departamento de Química, Universidad de Chile, Santiago, Chile

Correspondence
Katherine Paredes-Gil, Programa Institucional de Fomento a la Investigación, Desarrollo e Innovación, Universidad Tecnológica Metropolitana, Ignacio Valdivieso 2409, P.O. Box 8940577, San Joaquín, Santiago, Chile.
Email: k.paredesg@utem.cl

Funding information
Comisión Nacional de Investigación Científica y Tecnológica, Grant/Award Number: PAI77180024; Fondo Nacional de Desarrollo Científico y Tecnológico, Grant/Award Numbers: 1140503, 1150629, 1180158, 3170117

Abstract

Time-dependent density functional theory (TD-DFT)/periodic DFT calculations were performed to determine the role of pro-aromatic organic D-A-π-A type dyes (the NL1-NL17 family) with Thieno[3,4-b]pyrazine (Tpy) as A acceptor group into dye-sensitized solar-cells (DSSC). This work presents a discussion of the ground and excited states of these dyes along with the aromaticity analysis and the *electron injection* step using a dye@$(TiO_2)_{72}$ model. The results suggest that the pro-aromatic behavior increases from the thiophene ring to the pyrazine when an acceptor π-bridge such as phenyl is used. This strong pro-aromaticity is also reflected in the *electron injection* step, studied using a 3x2 3 layer $(TiO_2)_{72}$ slab model. The resulting adsorption energies (ΔE_{ads} and ΔG_{ads}) and the electron injection (ΔG_{inject}) in the stablest coordination mode, Bid_CN_COOH, indicate that the redox reaction (Dye* → $Dye^+ + e^-$) is stronger and more spon than the adsorption reaction ($Dye^+ + TiO_2$ [$+e^-$] → Dye@TiO_2) in the *electron injection*. In this way, the highest efficiency of NL6 and NL12 is a consequence of the more significant pro-aromatic characteristics and the more spontaneous redox process. Finally, these NL dyes are promising in the molecular engineering of D-A-π-A metal-free types dyes.

KEYWORDS
D-A-π-A dyes, metal-free organic dyes, pro-aromatic molecules, solar cell, TiO_2 surface

1 | INTRODUCTION

Dye-sensitized solar cell (DSSC)[1–3] are promising photovoltaic systems for the generation of electrical energy, currently reaching a record of 14% in the overall power conversion efficiency (η).[4,5] In DSSC, the dye harvests sunlight and becomes photoexcited, promoting the molecule to an excited state. This generates an electron with enough energy to escape and move toward the titanium dioxide surface (TiO_2) in a process known as *electron injection*.[6,7] The above injection, along with an electrolyte, creates an electrical circuit that powers a device. Three sensitizing's families have been reported: Ruthenium complexes, Zn-porphyrins and Metal-free organic sensitizers. Ruthenium complexes were proposed in 1991 by O ̀Regan and Grätzel.[8] The most prominent ones are N3 dye [$RuL_2(NCS)_2$],[9] and its protonated salt N719,[10,11] among others. Zn-porphyrins present broad and strong absorption in the visible region.[12,13] Among the most important ones there are YD-o-C8 (η = 12.3%),[14,15] SM371 (η = 12.0%), and SM315 (η = 13.0%).[16] Metal-free organic sensitizers[17] are generally used as junction systems or are co-sensitized[18] with two or more kinds of dyes to improve their efficiency. The most recent dye is the ADEKA-1 (η = 12.0%)[19] which, when co-sensitized with LEG4, increases the efficiency of up to 14%.[20]

Most current research has focused on the structural design of the dyes because their chemical characteristics control the yield of the solar cell. In general, the dyes traditionally have a donor-π-bridge-acceptor rearrangement (D-π-A) that favors the intramolecular charge transfer.[21–23] In this context, the donor-acceptor nature of the dyes is a popular discussion topic.[24] Some of the main structural changes include bulky donor groups, such as perylene in WW3-WW8,[25] and strong acceptor groups such as thiazole ligand in ZZXN7-ZZXN9,[26] among others. Nevertheless, to facilitate the electron transfer, W. Zhu et al. synthesized WS-1 and WS-2 dyes[27] which include 2,1,3-benzothiadiazole (BTD) as an auxiliary electron acceptor group (A), leading to the D-A-π-A rearrangement. This novel sensitizer type gives a photovoltaic cell performance of η = 8.0%, which is higher than L1 (η = 2.0%), the simplest D-π-A dye. Thus, the D-A-π-A rearrangement is nowadays the most common one in the architecture of new photosensitizers.[28,29] In this respect, the highest efficiency solar cell for the metal-free organic dyes is reached in SGT-130 (η = 10.47%),[30] while in Zn-porphyrins is SM315 (η = 13.0%).[16] Both dyes incorporate benzothiadiazole in their acceptor groups (A). Similar dyes have been synthesized in this manner, some of the most remarkable of which are RK-1, and RKF dyes with substituted benzothiadiazole, and indeno[1,2-b]-thiophene, which give overall efficiencies between 8.22% and 10.25%.[31,32] JZ117 and JZ145 dyes[33] with 5,6-difluro-2,1,3-benzothiadiazole have overall efficiencies of η = 7.4% and 9.1%, respectively. Furthermore, WS-5,[34] WS-9,[35] W7-W8,[36] KM10-KM11,[37] LC-6-LC-8,[38] and D1-D3[39] photosensitizers have also been synthesized. (See Figure 1 for representation).

It is observed that 2,1,3-benzothiadiazole corresponds to the auxiliary electron acceptor group (A) most employed in D-A-π-A type dyes.[40] However, quinoxaline and benzo[a]pyrazine are also used as acceptor groups in IQ-4[41] and YA422[21] dyes, respectively. These present a notable improvement in the overall efficiency of the cell, achieving values of 9.83% and 10.10%, respectively. Therefore, in recent years, the development of novel photosensitizers has been guided by chemical modifications to the acceptor group (A).[42] Prominent examples include, the PB1-2, DP1-2 dyes[43] with thieno[3,4-*b*]thiophene (TTh), and NL2-NL8 sensitizers[44] and FNE32-FNE34 dyes[45] with thieno[3,4-*b*]pyrazine derivatives (TPy) as auxiliary electron acceptor groups (A). Both groups, TTh and TPy, have a quinoidal resonance structure, which is stable when the dye is in an excited state (see Figure 2). This resonance structure in PB1-2 and DP1-2 dyes has been associated with a pro-aromatic behavior,[46] which is a consequence of the increasing aromaticity of the molecule when acquiring a diradical or zwitterion form. Moreover, these aromatic properties are related to wavelength shifts toward the near-infrared (NIR) and a decrease in the optical band gap and the back-electron transfer in the solar cell. Therefore, highly stable and pro-aromatic photosensitizers are a current challenge in the molecular engineering of metal-free D-A-π-A type dyes. Consequently, one of the objectives of this study is to investigate the pro-aromatic characteristics of thieno[3,4-*b*]pyrazine (A) into NL2-NL8 sensitizers.

On the other hand, it is important to highlight that computational studies allow the prediction and explanation of dyes´ outstanding properties.[47–49] Specifically, electronic spectra and gap energies are calculated to understand the *photoexcitation step*.[50–53] These are conducted through time-dependent density functional theory (TD-DFT), which identifies the orbital contributions of electronic states that participate in the electronic transition when absorbing UV-Vis light dye. The most employed functionals tested in these systems are hybrid and meta-hybrid-GGA, such as B3LYP,[54,55] CAM-B3LYP,[56] and M06.[16] Moreover, computational studies analyze the *electron injection step* in the solar cell, modeling the dye@TiO_2 interaction. This has been widely explored in recent years using the anatase (101) or rutile (110) TiO_2 surface. The most outstanding works study the adsorption of perylene[57] and other organic dyes.[58–60] Recent results demonstrate that a precise analysis of the chemical properties of dye@TiO_2 should be carried out using the PBE + D + U functional in periodic DFT calculations.[61–64] Therefore, an overall understanding of the two most important steps in the solar cell, the *photoexcitation* and *electron injection*, involving a set of novel D-A-π-A type dyes, will enable rational design of novel photosensitizers and their performance in DSSC.

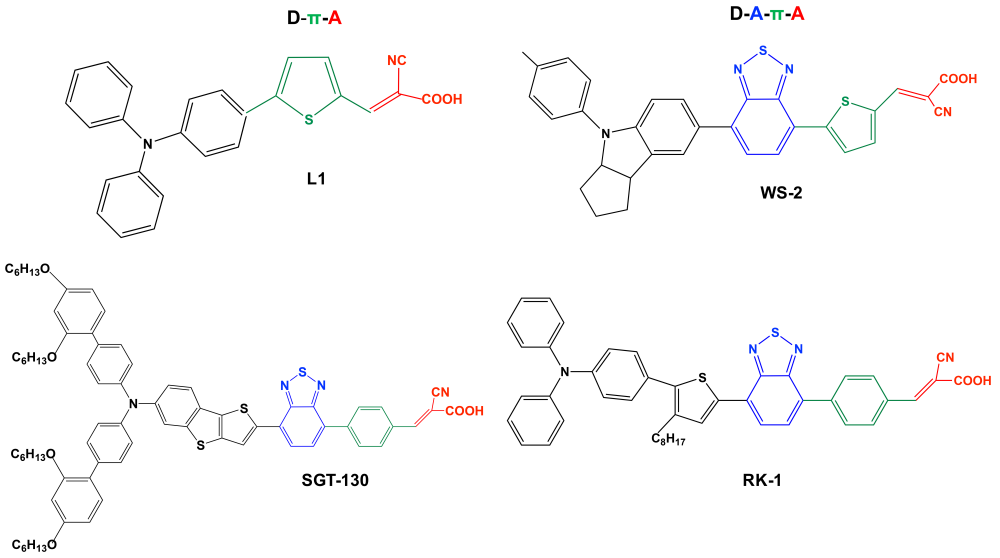

FIGURE 1 Some representative dyes with D-π-A and D-A-π-A rearrangements. In D-A-π-A type dyes, 2,1,3-benzothiadiazole is the acceptor group (A)

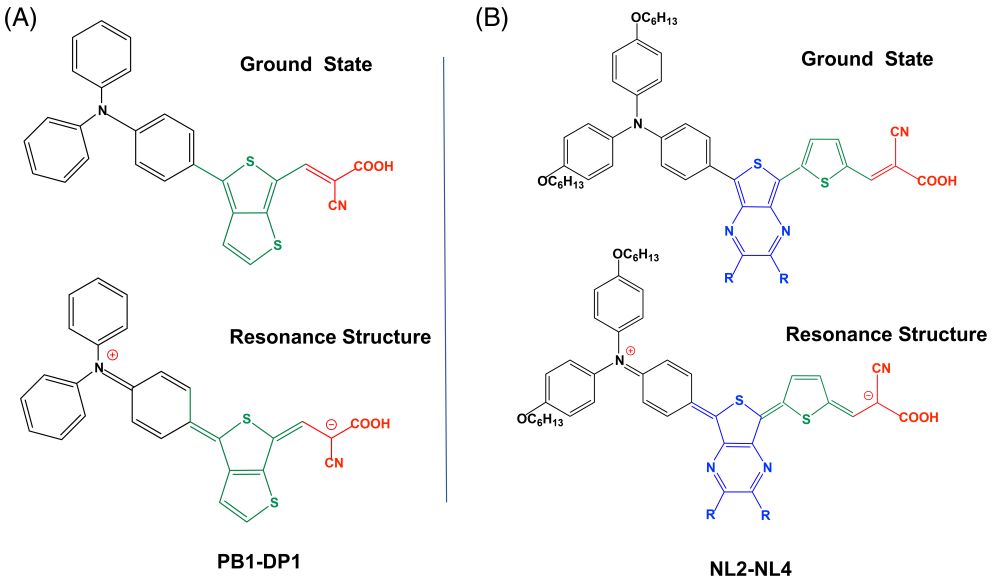

FIGURE 2 A, PB1-DP1 and B, NL2-NL4 dyes in ground and excited states. The excited states present a resonance structure with quinoidal and zwitterionic forms. In B, NL2-NL4 dyes are 2,3- substituents on the pyrazine ring, so: R = CH_2CH_3 for NL2, R = Ph for NL3, and R = *p*-methoxy-phenyl for NL4

Finally, this work aims to extend the study of pro-aromatic organic compounds with thieno[3,4-b]pyrazine (NL2-NL8) as the electron acceptor group (A) toward other similar metal-free sensitizers, in order to novel potential dyes. For this purpose, a computational study was carried out on a set of dyes called NL1-NL17. Moreover, the goal of this study is to also gain insight into the role of the acceptor groups, thiophene (Th), benzothiadiazole (BTD), thieno[3,4-*b*]thiophene (TTh) and thieno[3,4-*b*]pyrazine (Tpy) on the L1, SGT-130, PB1, and NL dyes, respectively, to determine the relationship between the chemical properties and the performance of the solar cell. We expect to provide new knowledge in the DSSC field.

2 | MODELS AND COMPUTATIONAL DETAILS

2.1 | MODELS

The NL1-NL17 dye structures are described in Figure 3 and Table 1. Herein, NL2-NL8 dyes correspond to the photosensitizer previously reported,[44] while NL1, NL9-NL17 are in silico designed dye structures. Specifically, modifications are made inside the four blocks of the D-A-π-A rearrangement: donor (D), acceptor (A), π-bridge (π) and anchoring group (A). In general, the (D) groups evaluated are the indolizine group (Ind) and the triphenylamine derivatives (TPA). The (A) groups studied are thieno[3,4-*b*]pyrazine (TPz) in NL1, and 2,3-di-substitued-thieno[3,4-*b*]pyrazine (2,3-di-TPz) in the others. The π-bridges (π) used are the thiophene (Thio), phenyl (Ph), pyridine (Py), and pyrazine (Pz) groups. Last, the anchoring groups (A) involved in this work are, the carboxylic acid, RCOOH, and the cyanoacrylic acid, $RCH_2CCNCOOH$.

2.2 | COMPUTATIONAL DETAILS

The calculations for the NL1-NL17 dyes were performed within the framework of DFT[65] using the GAUSSIAN 09[66] program. Optimization geometries and vibrational analysis were done using the B3LYP + D3[67,68] exchange-correlation functional, which incorporated Grimme's dispersion correction. Also, the 6-31 + G(d,p) basis set[69] was used to describe the carbon, hydrogen, nitrogen, oxygen, and sulfur atoms. Dichloromethane solvent was included in the optimization geometries of NL1-NL17 dyes through the continuum solvation model (SMD).[70] Thermal contributions (1 atm and 298 K) to enthalpy and Gibbs energy were evaluated using the harmonic oscillator and rigid rotor model as it was implemented in the Gaussian 09 program. The atomic charges were obtained with the natural population analysis (NPA) of Weinhold et al.[71]

To calculate the UV-Vis absorption spectra of the NL1-NL17 dyes, the lowest 40 excitation energies were computed using TD-DFT.[72] These were performed with the exchange-correlation functionals, B3LYP-D3,[73] CAM-B3LYP,[74,75] and M06,[76] already widely tested in the prediction of electronic spectra, using dichloromethane (DCM) as a solvent through the continuum solvation model (SMD).

Nucleus-independent chemical shifts (NICS)[77] were obtained in the Amsterdam Density Functional (ADF)[78–80] code for calculating NMR shielding values with the gauge-independent atomic orbital (GIAO) method.[81] In addition, the generalized gradient approximation BP86 functional[82–84] and the Slater-type-orbital[85] (STO) basis set with triple-ζ quality double plus polarization functions (TZ2P) were used for all atoms. Specifically, the shielding tensor isotropic value σ_{iso} and the *z*-axis components σ_{zz} were scanned over distances r ranging from −3.0 to 3.0 Å along the line, perpendicular to the plane of rings 1-2 of the thieno[3,4-b]pyrazine, and of ring 3 in the π-bridge group, on the NL1-NL17

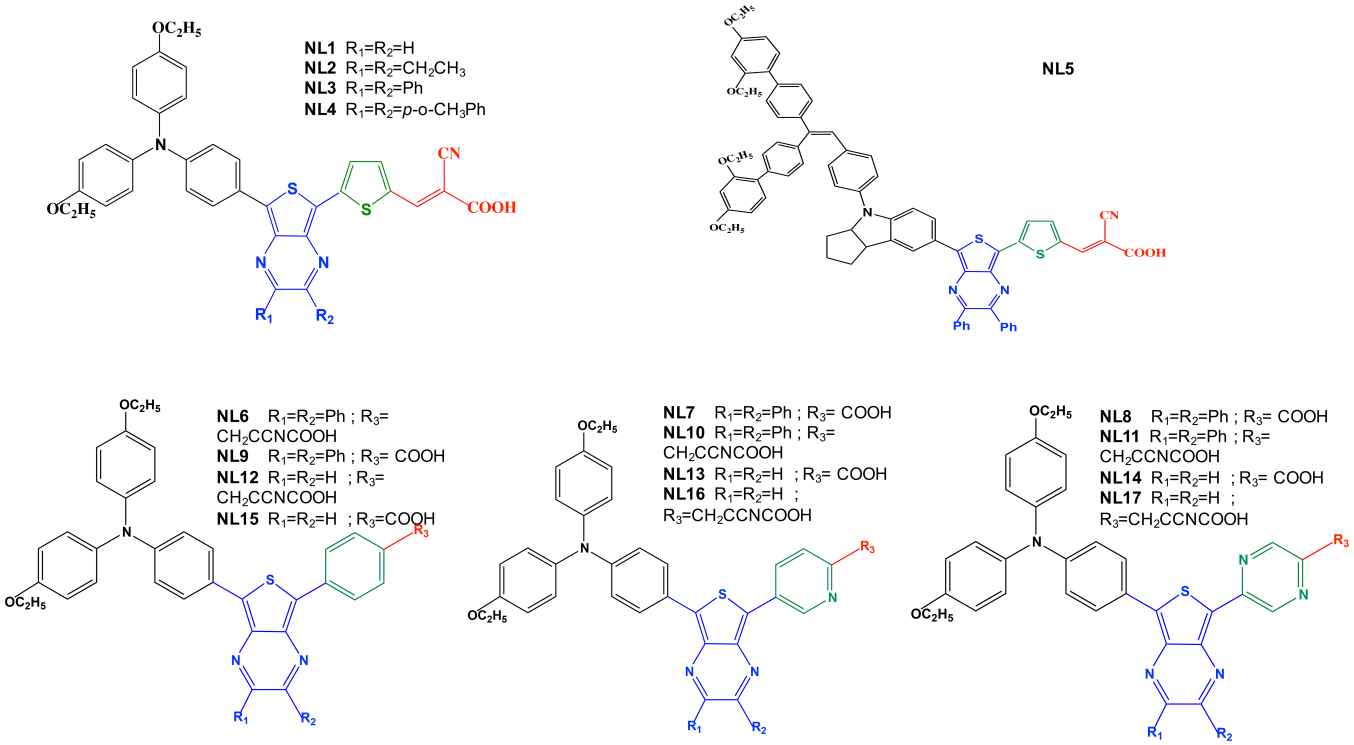

FIGURE 3 The structures of NL1-NL17 dyes with 2,3-di-susbtituted-thieno[3,4-b]pyrazine (2,3-di-TPz) as the auxiliary electron acceptor group (A)

TABLE 1 Donor (D), acceptor (A), π-bridge (π) and anchoring groups (A) in the NL1-NL17 dyes with D-A-π-A rearrangement

Dyes	Donor (D)	Acceptor 2,3-di-substitued-TPy (A)	π-bridge (π)	Anchoring (A)
NL1	TPA	$R_1 = R_2 = H$	Thiophene	$-CH_2CNCOOH$
NL2	TPA	$R_1 = R_2 = CH_2CH_3$	Thiophene	$-CH_2CNCOOH$
NL3	TPA	$R_1 = R_2 = Ph$	Thiophene	$-CH_2CNCOOH$
NL4	TPA	$R_1 = R_2 = p\text{-}OCH_3Ph$	Thiophene	$-CH_2CNCOOH$
NL5	Ind	$R_1 = R_2 = Ph$	Thiophene	$-CH_2CNCOOH$
NL6	TPA	$R_1 = R_2 = Ph$	Phenyl	$-CH_2CNCOOH$
NL7	TPA	$R_1 = R_2 = Ph$	Pyridine	$-CH_2CNCOOH$
NL8	TPA	$R_1 = R_2 = Ph$	Pyrazine	$-CH_2CNCOOH$
NL9	TPA	$R_1 = R_2 = Ph$	Phenyl	−COOH
NL10	TPA	$R_1 = R_2 = Ph$	Pyridine	−COOH
NL11	TPA	$R_1 = R_2 = Ph$	Pyrazine	−COOH
NL12	TPA	$R_1 = R_2 = H$	Phenyl	$-CH_2CNCOOH$
NL13	TPA	$R_1 = R_2 = H$	Pyridine	$-CH_2CNCOOH$
NL14	TPA	$R_1 = R_2 = H$	Pyrazine	$-CH_2CNCOOH$
NL15	TPA	$R_1 = R_2 = H$	Phenyl	−COOH
NL16	TPA	$R_1 = R_2 = H$	Pyridine	−COOH
NL17	TPA	$R_1 = R_2 = H$	Pyrazine	−COOH

metal-free organic dyes (Figure 4). These NICS scans were able to provide a measurement of the aromatic, non-aromatic, or antiaromatic behavior on the rings of these molecules, through the shapes curves analysis and the isotropic value at distance *r*. Negative values isotropic are associated to aromaticity, while positive values to antiaromaticity.[86] In this context, the NICS analysis might identify the pro-aromatic behavior of the NL1-NL17 metal-free organic dyes and the relationship between structure, aromaticity, and sensitizer function. It is essential to highlight that the NICS analysis for NL1-NL17 dyes has only been realized in a ground state because regrettably, the TD-DFT magnetic shielding tensor is not available for the excited state.

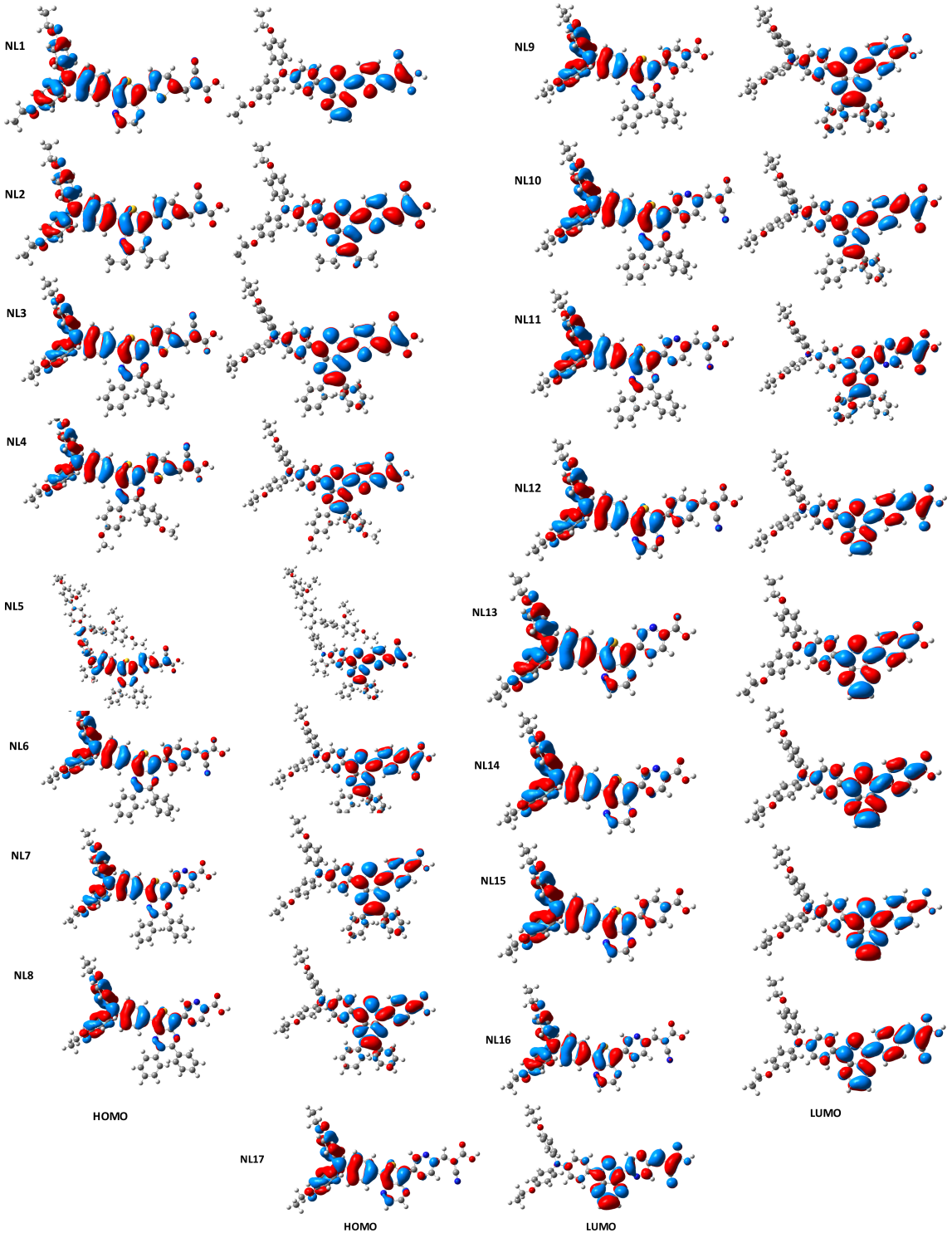

FIGURE 4 Molecular orbitals (HOMO-LUMO) associated with the most intense electronic transitions for NL1-NL17 dyes in the solvent phase of the GAUSSIAN program

Furthermore, all the calculations for dye@TiO_2 were performed using the periodic density functional theory approach implemented in the Vienna Ab-initio Simulation Package, VASP 5.2.[87–89] The PBE[90] GGA exchange-correlation functional was chosen due to the cost-efficiency ratio reported for many extended systems.[91] Grimme[68] and Hubbard[92] empirical terms were also included for the dispersion and the wrong insulator behavior (PBE + D + U) correction, respectively. The Hubbard term incorporated the effective U potential described by Anisimov and co-workers,[93] where U = 5.8 eV for the Ti(3d) and O (2p) bands. This reproduced the semiconductor behavior,[94] and agreed with other U values that predicted a correct behavior experimentally. Additionally, the valence electrons were expanded in a plane wave basis set with the

Monkhorst-Pack grid centered at Γpoint (1 1 1)[95] and a cutoff of 500 eV for the kinetic energy. The core electrons were described through the projector augmented wave (PAW) pseudopotentials.[96,97]

The 3 × 2 3 layer $(TiO_2)_{72}$ slab model for the TiO_2 anatase (101) surface was built with cell parameters of 11.424 x 20.866 x 35.0 Å. These parameters were chosen based on the size of the dyes and empty space of 10 Å in *c*, added to avoid any interaction among the fictitious replica when the slabs were periodically replicated. The dye@$(TiO_2)_{72}$ studied corresponds to: (a) Bid_CN_COOH, the stablest coordination mode reported,[58,98,99] and the most commonly analyzed in the literature, (b) Bid_COO_H, and (c) Mono_COOH monodentate and bidentate coordination modes, respectively.[100,101] Therefore, the slab model $(TiO_2)_{72,}$ and the (NL1,NL6,NL7,NL8,NL15)@$(TiO_2)_{72}$ models were fully optimized using ISIF = 3, while the isolate L1, SGT-130, PB1, and NL dyes using ISIF = 2. Also, the relaxation of geometry was considered converged when the energy difference with respect to the previous optimization step was less than 1 x 10^{-5} eV, and the SCF tolerance was 1 x 10^{-6} eV.

Moreover, the vibrational frequencies were computed by numerical differentiation of the analytical first derivatives using the central difference formula, which involved two displacements for each atom in each direction. In this Hessian matrix, only the dyes and the first layer of the surface were considered. This methodology confirmed that the optimized structures were minimal, and enabled the calculation of the free energy G at T = 298.15 K. For this purpose, a script was used,[102] which calculated the quasi-harmonic thermochemical corrections. Specifically, the entropy S was computed in terms of the vibrational (harmonic oscillator approximation) and rotational (quasi-RRHO approach) entropies, in addition to a damping function, as it has been described by Grimme,[103] while the enthalpy H was obtained through $H = U + PV$, where P was given by the total energy change in function of the volume cell optimized.

The adsorption energies with correction for the lateral interactions[104] ($\Delta E_{ads} + \Delta E_L$), the adsorption free energies (ΔG_{ads}), and the free electron injection energies (ΔG_{inject}) were studied. Specifically, the adsorption energies[105,106] (ΔE_{ads}) and the free energies (ΔG_{ads}) of dye@TiO_2 were calculated from the ground state total energy of the fully optimized species as:

$$\Delta E(G)_{ads} = E(G)(\text{dye@TiO}_2) - [E(G)(\text{TiO}_2) + E(G)(\text{dye})] \quad (1)$$

where $E(G)$(dye@TiO_2) is the energy (free energy) of the dye in the TiO_2 surface, $E(G)(TiO_2)$ is the energy (free energy) of the isolated surface, and $E(G)(dye)$ is the energy (free energy) of the isolated dye. The correction for the lateral interactions is defined as:

$$\Delta E_L = E_{\text{dye at } 30\times30\times30} - E_{\text{dye at } 11\times20\times35} \quad (2)$$

where $E_{\text{dye at } 30\times30\times30}$ is the energy of the dye is a cell of dimension 30 × 30 × 30 Å and $E_{\text{dye at } 11\times20\times35}$ is the energy of the dye in the same a, b, c cell of the dye@$(TiO_2)_{72}$ system.

The free electron injection energies (ΔG_{inject}) was based on the definition given by Matthews et al.[107] which proposed that the electron injection is a charge transfer reaction. It was defined by Katoh[108,109] as the energy difference resulting from the energy of the LUMO of the dye and the injection of an electron into the conduction band of the TiO_2, so:

$$\Delta G_{inject} = E^{dye}_{LUMO} - E^{TiO_2}_{CB} \quad (3)$$

In that sense, the electron injection step was considered within two stages, a redox (Dye* → $Dye^+ + e^-$) and an adsorption reaction (Dye^+ + TiO_2 [+e^-] → Dye@TiO_2). Therefore, the redox free energy (ΔG_{redox}) contribution was obtained from the adsorption free energy (ΔG_{ads}) and the free electron injection energies (ΔG_{inject}).

Finally, the projected density of states (PDOS) was obtained to understand the contributions of the different orbitals in a band, as it was implemented in VASP.

3 | RESULTS AND DISCUSSION

The results are divided into the following sections: (a) The electronic characterization and UV-Vis absorption spectra of the metal-free organic sensitizers, NL1-NL17, to gain insight into their behavior as light harvesters. (b) The aromaticity analysis of NL1-NL17, using the NICS concept. (c) The *electron injection* step of the most critical dyes of this family, through structural, energetic, and electronic analysis of the dye@$(TiO_2)_{72}$ systems. (d) The modeling of the L1@$(TiO_2)_{72}$, SGT-130@$(TiO_2)_{72}$, and PB1@$(TiO_2)_{72}$ systems, in order to comprehend the role of different acceptor groups inside the D-A-π-A rearrangement. Based on all of the above, this study aimed at understanding the chemical behavior of the NL2-NL8 dyes in the solar cell, to predict the performance of the new dyes proposed in DSSC, and to contribute to the rational design of novel dyes with high overall power conversion efficiency (η).

3.1 | NL1-NL17 metal-free sensitizers: Electronic characteristics of the ground and excited states

The NL1-NL17 metal-free sensitizers are generally planar structures with two branches coming from the bulky donor group (D). Some geometrical parameters are depicted in Figure S1 of the Supporting Information (SI) and show that these molecules are similar in planarity to a great variety of dyes.[110] This structural characteristic is fundamental for designing dye because it quickly promotes the movement of electrons toward the anchoring group. Noticeably, the structural and electronic features of the metal-free organic dyes could be related to their efficiency when sensitized. Hence, the natural atomic charge of the main fragments of the NL1-NL17 dyes (Q_{Donor}, $Q_{Acceptor}$, $Q_{\pi\text{-bridge}}$ and $Q_{Anchoring}$) is analyzed to study the intramolecular charge transfer effects, which, along with the electronic transitions, are responsible for the *photoexcitation step*. The results are described in Table 2.

These results show that the donor D and the anchoring A groups are solely electron donors and electron acceptors, respectively, while the acceptor A and π-bridge groups do not have a predominant character. Specifically, the dyes with the most accepting anchoring groups A are NL1-NL5, which have thiophene as the π-bridge, while NL7, NL8, NL9, NL13, NL14, and NL15 are the least electron deficient ones.

Moreover, the 2,3-di-substitued-thieno[3,4-*b*]pyrazine (A = 2,3-di-TPz) are electron deficient (NL1, NL6-NL9, NL12-NL16) when the π-bridge has a donor or slightly acceptor nature. These results are significant because they shed light on the structure-performance relationship. In this way, NL6, which has the highest power conversion efficiency (PCE = 7.08%), has an electron deficient 2,3-di-TPz, an electron rich π-bridge, and a high electron accepting anchoring group. Meanwhile, NL7 and NL8, with have the lowest PCE (0.83% and 0.89%, respectively), have an anchoring group with weak acceptor character. Therefore, the electron deficiency of the 2,3-di-TPz (A) and acceptor nature of the anchoring group (A) could be related to the performance of the solar cell.

To understand the chemical nature of the NL1-NL17 photosensitizer, the change in the natural atomic charges of the anchoring groups ($\Delta Q_A = Q_{A\_CNCOOH} - Q_{A\_COOH}$) are analyzed when the π-bridge and the acceptor group are substituted (NL6 vs NL9; NL7 vs NL10; NL8 vs NL11; NL12 vs NL15; NL13 vs NL16; NL14 vs NL17). Also, this study examines the $\Delta Q_{\pi\text{-bridge}}$ ($\Delta Q_{\pi\text{-bridge}} = Q_{\pi\text{-bridge\_thio}} - Q_{\pi\text{-bridge\_Ph/Py/Pz}}$) defined as the change in the atomic charges when the π-bridge varies from thiophene to phenyl, pyridine and pyrazine. (NL1 vs NL12; NL1 vs NL13; NL1 vs NL14; NL3 vs NL6; NL3 vs NL7; NL3 vs NL8). Finally, the $\Delta Q_{bulky\text{-}A}$ ($\Delta Q_{bulky\text{-}A} = Q_{bulky\text{-}A\_Ph} - Q_{bulky\text{-}A\_H}$) is obtained to analyze the bulky substituent effect on the acceptor group 2,3-di-TPz (A) when $R_1 = R_2 =$ Ph is replaced by $R_1 = R_2 =$ H (NL6 vs NL12; NL7 vs NL13; NL8 vs NL14; NL9 vs NL15; NL10 vs NL16; NL11 vs NL17). The results are described in Table 3 and show that if the anchoring group cyanoacrylic is replaced by carboxylic acid (ΔQ_A), a less donor character is obtained. This is higher when the π-bridge is a phenyl group and is lower when the π-bridge donor type is employed. This is the ideal behavior, because a potential electron deficient anchoring group will allows an easy electron injection to the TiO_2 surface.

Moreover, $\Delta Q_{\pi\text{-bridge}}$ shows that if the thiophene is substituted by Ph, Py, or Pz, a donor effect will be achieved. Therefore, in the experimentally reported NL2-NL8 dyes, it is observed that the lowest donor character in the π-bridge is associated with the higher PCE ($\Delta Q_{\pi\text{-bridge}} = 0.037$ for NL3 vs NL6). When NL1 is compared to NL12, a low donor character is found, so that the proposed NL12 dye becomes a potential

TABLE 2 Natural atomic charges (*Q*) associated with the main fragments of the NL1-NL17 metal-free sensitizers

Dyes	Q_{Donor}	$Q_{Acceptor}$	$Q_{\pi\text{-bridge}}$	$Q_{Anchoring}$
NL1	0.157	−0.006	0.089	−0.234
NL2	0.131	0.036	0.084	−0.252
NL3	0.146	0.011	0.087	−0.245
NL4	0.137	0.033	0.083	−0.254
NL5	0.102	0.034	0.091	−0.227
NL6	0.120	−0.001	0.050	−0.168
NL7	0.107	−0.023	−0.073	−0.011
NL8	0.118	−0.001	−0.114	−0.003
NL9	0.087	−0.029	−0.041	−0.016
NL10	0.138	0.009	−0.004	−0.144
NL11	0.161	0.031	−0.058	−0.134
NL12	0.119	−0.016	0.055	−0.158
NL13	0.111	−0.032	−0.070	−0.010
NL14	0.122	−0.016	−0.106	−0.002
NL15	0.091	−0.039	−0.037	−0.015
NL16	0.140	−0.009	0.002	−0.134
NL17	0.156	0.009	−0.044	−0.121

TABLE 3 Electronic effect of the anchoring, π-bridge, and 2,3-di-substitued-TPz groups in the NL1-NL17 metal-free sensitizers

π-bridge/bulky-A or A	Anchoring effect ΔQ_A ($R_1 = R_2$ = Ph)/($R_1 = R_2$ = H)[a]	π-bridge effect $\Delta Q_{\pi\text{-bridge}}$ ($R_1 = R_2$ = H)/($R_1 = R_2$ = Ph)[a]	Bulky TPz effect $\Delta Q_{\text{bulky-A}}$ (R_3 = –CNCCOOH)/(R_3 = COOH)[b]
Phenyl	−0.152/−0.144	0.034/0.037	0.014/0.010
Pyridine	−0.133/−0.124	0.087/0.091	0.018/0.008
Pyrazine	−0.131/−0.119	0.134/0.145	0.022/0.015

[a]If bulky-A is fixed.
[b]If A is fixed.

photosensitizer. Additionally, $\Delta Q_{\text{bulky-A}}$ shows that there are no essential changes when the 2,3-diphenyl-Tpz or the TPz are used as the acceptor group. Therefore, in the dye design of the NL family, the bulky substituent effect is not important. This is also observed when Q_{Acceptor} is compared in NL1-NL4, demonstrating that the donor-acceptor substitution in the 2,3-di-TPz does not cause significant changes to the chemical reactivity of these molecules.

Following the electronic characterization of the dyes, the band gap is calculated based on the HOMO(H) and LUMO(L) energy levels. The results for the reported dyes NL2-NL8 are depicted in Figure S2, while the band gap for the other metal-free organic dyes, NL1, and NL9-NL17 are described in Figure S3 of the SI. In the former, the gap energies obtained agree with the values reported experimentally for the dye optical band gaps. For the new dyes proposed, the band gap is between 1.8 and 2.1 eV. The high gap energies correspond to NL13, NL14 and NL9, NL15. These have pyridine, pyrazine and phenyl as the bridge, respectively, and carboxylic acid as the anchoring group, while the narrow gap is obtained in NL1, NL10-NL12, NL16, and NL17, which have cyanoacrylic acid as the common anchoring group. Therefore, the results show that the LUMO energies for dyes with carboxylic acid, as the anchoring group, are lower than the LUMO energies for dyes with cyanoacrylic acid. These results are significant, because together with the stronger acceptor character of the cyanoacrylic acid, they explain the best behavior of these anchoring groups in the electron injection step inside solar cells.

Conversely, the electronic characterization of the excited state of the metal-free sensitizers NL1-NL17 is performed through the TD-DFT framework using the B3LYP-D3, M06 and CAM-B3LYP functional and the 6-31G(d,p) basis set for all atoms. Tables S1, and S2 of the SI, and Table 4, respectively, describe the wavelength (λ), oscillator strength (f) and assignments of the most important electronic transitions calculated in the solvent phase. The results obtained show that in NL2-NL8 dyes, the maximum wavelengths calculated are overestimated when the B3LYP-D3 and M06 functional are used. Nevertheless, they have reproduced accurately when CAM-B3LYP is employed. Table 5 compares these maximum wavelengths, the experimental values, and the levels reported to B3LYP/6-311G(d,p).[44] As can be observed, the maximum wavelengths decrease in the order B3LYP-D3 > M06 > CAM-B3LYP functional.

In addition, considering the results in Table 4, two wavelengths types can be observed in all the NL1-NL17 sensitizers. The first bands extend to the infrared region (≈600 nm), and the second corresponds to the visible light region (300-400 nm). The red-shift wavelengths are the most intense transitions and involve the frontier orbitals HOMO(H)-LUMO(L). In general, these HOMOs are π orbitals localized in the phenyl groups of the donor group (D) and the thiophene of the acceptor (A), while the LUMOs present electronic density over the anchoring groups (A). (See Figure 4) This charge transfer is essential for the successful behavior of the molecules as dyes, since they have always been obtained in many molecules synthesized as sensitizers. Furthermore, these dyes are novel because they can absorb a photon and generate thermal energy as consequence of changes in their vibrational states. This energy could also be transformed into electrical energy, increasing the solar cell performance. In this manner, NL1, NL10, and NL12 have longer wavelengths and broader bands, while NL7, NL8, NL13, and NL14 have shorter wavelengths. Therefore, the dyes with high donor character in the π-bridge show a decrease in the red-shift wavelengths.

The bands between 300 and 400 nm correspond in general to electronic transitions from H − 1 to L and H to L + 1 orbitals. However, in some dyes such as NL7 and NL8, the inner orbitals H-8, and H-6, participate in the electronic transitions, making the withdrawal of the excited electron more difficult. This also explains the low overall efficiency of these sensitizers. Other dyes with inner orbitals participating in electronic transitions in the visible region are NL9 and NL13. Therefore, the results of this study also predict that these two sensitizers could present a low overall efficiency.

3.2 | The aromaticity analysis of the NL1-NL17 photosensitizers

In order to gain further insight into the aromaticity of the NL1-NL17 photosensitizers, NICS scans are performed on the acceptor group (A), thieno[3,4-b]pyrazine (ring 1 and 2), and on the π-bridge groups (ring 3) (See Figure 5). The results for the NL1, NL6, NL9, and NL12 dyes are presented in Figure 6, and the results for the others ones are shown in Figures S4-S6. Moreover, Table 6 tabulates single isotropic σ_{iso} and z-axis components σ_{zz} NICS values, which are taken in the inflection points of the curve to complement the aromaticity discussion. In all the sensitizers studied, the curve shape is found to correspond to aromatic systems. Minimum values for σ_{zz} are obtained near to the center of the rings (between r = −1 and 1), indicating that, in this position, the aromatic character is at its maximum, while long distances decrease as a consequence

TABLE 4 Calculated wavelength (nm), oscillator strength (f), and origin of the electronic transitions for the NL1-NL17 dyes using TD-DFT in the solvent phase (CAMB3LYP functional) in the GAUSSIAN program

Dyes	λ (calc.)	*f*	Origin		Assignments	
NL1	622	1.441	H	L	D-A(TPz)	A(TPz)-π-A
	409	0.288	H – 1	L	D-A-π-A	A(TPz)-π-A
	396	0.123	H – 1	L	D-A-π-A	A(TPz)-π-A
NL2	589	1.580	H	L	D-A(TPz)	A(TPz)-π-A
	398	0.238	H – 1	L	D-A-π-A	A(TPz)-π-A
	376	0.059	H	L + 1	D-A(TPz)	A(TPz)-π
NL3	631	1.303	H	L	D-A(TPz)	A(TPz)-π-A
	423	0.493	H	L + 1	D-A(TPz)	A(Ph)-π
	402	0.180	H – 1	L	D-A-π-A	A(TPz)-π-A
NL4	628	1.314	H	L	D-A(TPz)	A(TPz)-π-A
	432	0.625	H – 1	L	D-A-π-A	A(TPz)-π-A
	401	0.247	H	L + 1	D-A(TPz)	A(TPz)-π-A
NL5	568	0.119	H	L	D-A(TPz)	A(TPz)-π-A
	464	0.211	H – 2	L	D	A(TPz)-π-A
	394	0.272	H	L + 1	D-A(TPz)	A(Ph)-π-A
NL6	574	1.161	H	L	D-A(TPz)	A(TPz)-π-A
	392	0.646	H	L + 1	D-A(TPz)	A(Ph)-π-A
	383	0.179	H – 1	L	D-A-π-A	A(TPz)-π-A
NL7	544	0.808	H	L	D-A(TPz)	A(TPz)-π-A
	369	0.248	H – 1	L	D-A-π-A	A(TPz)-π-A
	354	0.064	H – 8	L	A(Ph)	A(TPz)-π-A
NL8	533	0.886	H	L	D-A(TPz)	A(TPz)-π-A
	573	0.127	H – 1	L	D-A-π-A	A(TPz)-π-A
	359	0.266	H – 6	L	A(Ph)-π	A(TPz)-π-A
NL9	537	0.744	H	L	D-A(TPz).	A(TPz)-π-A
	373	0.222	H – 1	L	D-A-π-A	A(TPz)-π-A
	353	0.101	H – 7	L	A(Ph)-π	A(TPz)-π-A
NL10	583	1.190	H	L	D-A(TPz)	A(TPz)-π-A
	399	0.643	H	L + 1	D-A(TPz)	A(Ph)-π-A
	387	0.105	H – 1	L	D-A-π-A	A(TPz)-π-A
NL11	585	1.330	H	L	D-A(TPz)	A(TPz)-π-A
	402	0.596	H	L + 1	D-A(TPz)	A(Ph)-π-A
	390	0.039	H – 1	L	D-A-π-A	A(TPz)-π-A
NL12	560	1.267	H	L	D-A(TPz)	A(TPz)-π-A
	377	0.492	H	L + 1	D-A(TPz)	A(Ph)-π-A
	374	0.048	H – 1	L	D-A-π-A	A(TPz)-π-A
NL13	525	0.902	H	L	D-A(TPz)	A(TPz)-π-A
	357	0.072	H – 1	L	D-A-π-A	A(TPz)-π-A
	356	0.015	H – 6	L	A(Ph)-π	A(TPz)-π-A
NL14	521	0.985	H	L	D-A(TPz)	A(TPz)-π-A
	366	0.003	H – 4	L	π	A(TPz)-π-A
	354	0.044	H – 1	L	D-A-π-A	A(TPz)-π-A
NL15	522	0.857	H	L	D-A(TPz)	A(TPz)-π-A
	360	0.052	H – 1	L	D-A-π-A	A(TPz)-π-A
	355	0.030	H – 6	L	π	A(TPz)-π-A

(Continues)

TABLE 4 (Continued)

Dyes	λ (calc.)	f	Origin		Assignments	
NL16	565	1.304	H	L	D-A(TPz)	A(TPz)-π-A
	384	0.369	H	L + 1	D-A(TPz)	A(Ph)-π-A
	375	0.081	H – 1	L	D-A-π-A	A(TPz)-π-A
NL17	569	1.392	H	L	D-A(TPz)	A(TPz)-π-A
	386	0.303	H	L + 1	D-A(TPz)	A(Ph)-π-A
	378	0.036	H – 1	L	D-A-π-A	A(TPz)-π-A

TABLE 5 Experimental (exp), reported (A), and calculated (b-d) maximum wavelengths (λ_{max}) for the NL2-NL8 metal-free sensitizers

Dyes	λ_{max} (exp)	λ_{max} (a)	λ_{max} (b)	λ_{max} (c)	λ_{max} (d)
NL2	621	688	753	699	589
NL3	651	722	818	759	631
NL4	657	713	807	750	628
NL5	672	744	689	645	568
NL6	605	708	776	712	574
NL7	589	682	726	671	544
NL8	628	674	727	667	533

Notes: Values are in nm. (a) B3LYP/6-311G(d,p) (b) B3LYP+D3/6-31G(d,p); (c) M06/6-31G(d,p); (d) CAM-B3LYP/6-31G(d,p).

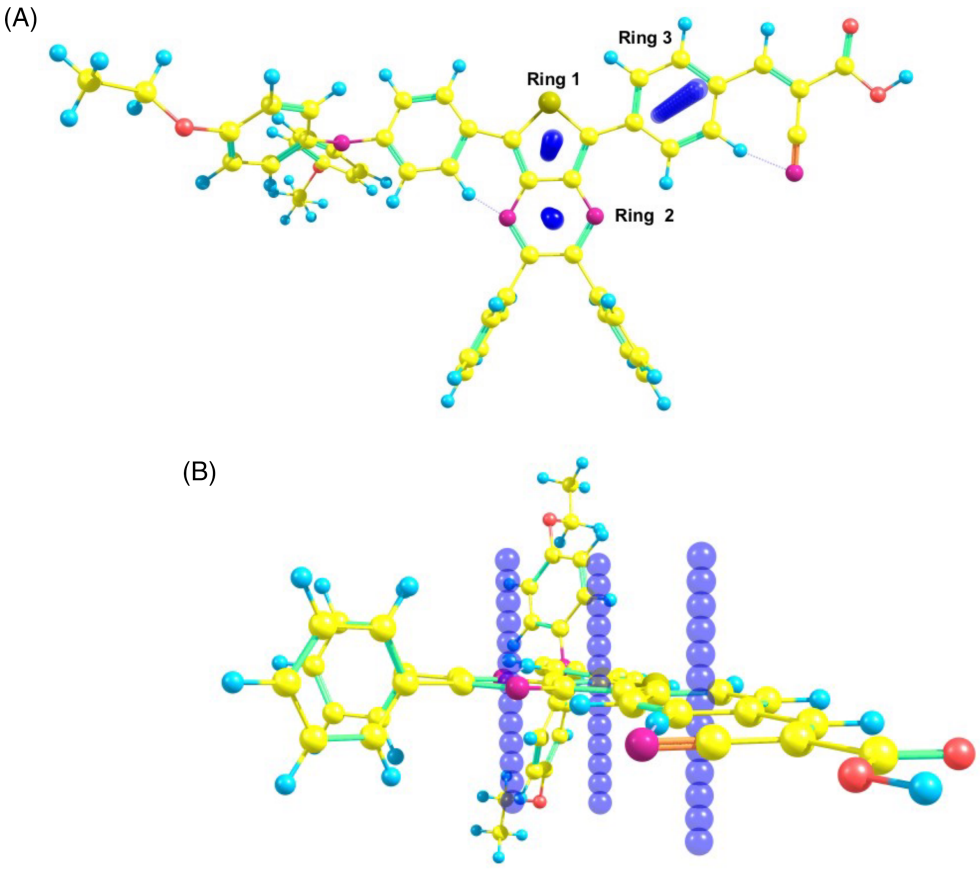

FIGURE 5 Rings and dummy atoms for NICS analysis on the NL6 dye. Two different positions of the molecule, A and B, are depict for clarity. For the other dyes, the NICS analysis was realized in the same way

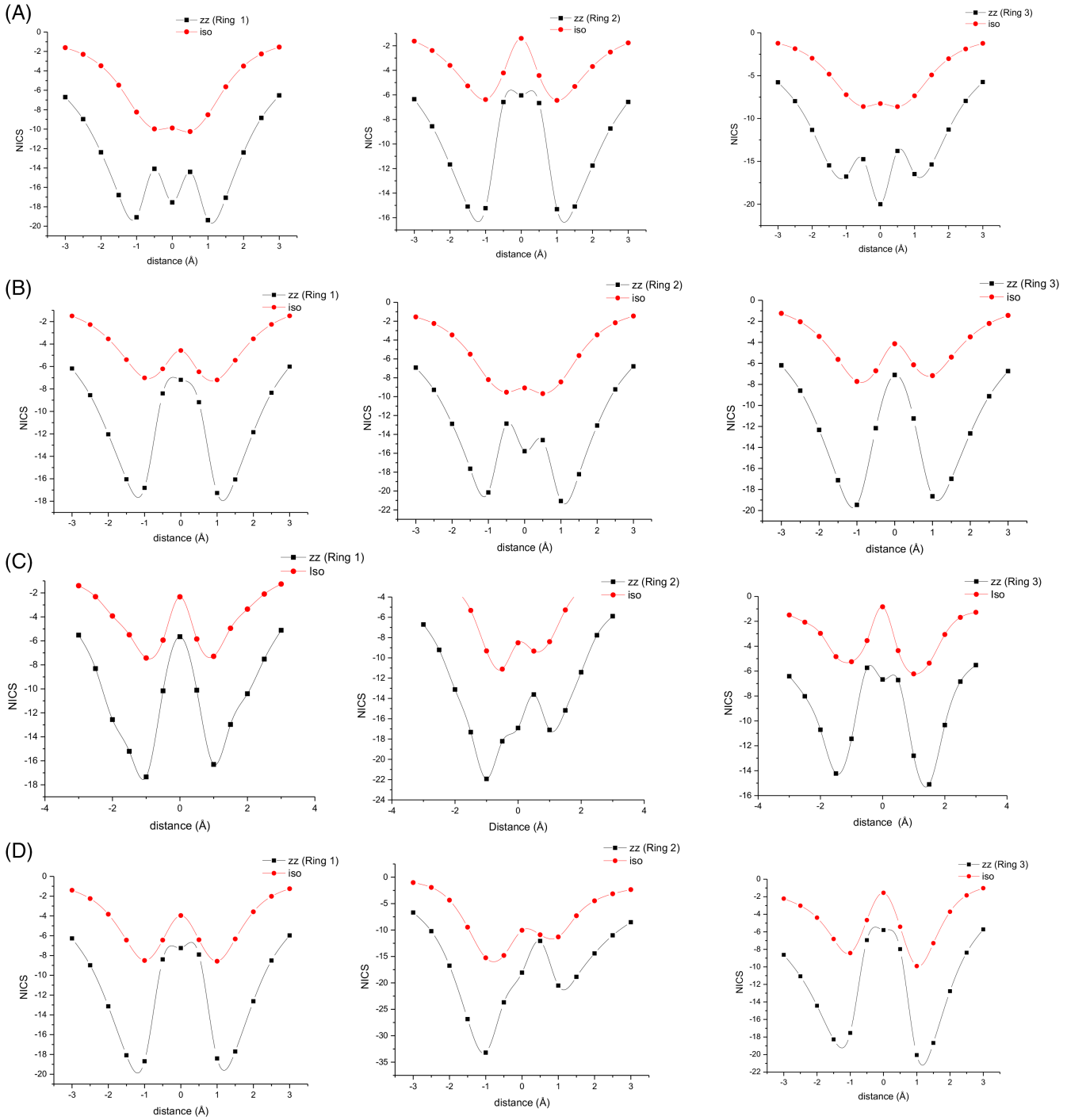

FIGURE 6 NICS values (ppm) as a function of distance (angstrom) in rings 1, 2, and 3 of four outstanding metal-free sensitized dyes: A, NL1; B, NL6; C, NL9; and D, NL12

of the π-cloud. Also, σ_{iso} is, in general, a soft curve representative of the average of the chemical shielding tensor. However, in some dyes, a maximum value is found at $r = 0$, indicating the lowest aromaticity level is reached in the center of the ring. Specifically, ring 1, a thiophene fused group, has to $r = -1$ and 1 σ_{zz} average values between −23.12 and −16.82 for NL5 and NL11, respectively. These near values showed similar aromatic behavior, indicating that the current of the neighboring rings does not have a significant influence on the local aromaticity. However, slight differences are found in the σ_{iso} values for NL1-NL5 and NL6-NL17 dyes, at $r = 0$. The first one shows aromaticity close to −9 ppm, while the last one between −5.91 and −1.36 ppm, which shows that in the center of the ring the aromaticity increases when the neighboring π-bridge is also thiophene. Ring 2, a pyrazine fused group, is highlighted by presenting an increase of aromaticity compared to ring 1 in the NL5-NL17 dyes, giving the highest σ_{zz} average values of −33.35, −36.14, and −32.12 ppm in the NL12, NL14, and NL17 dyes, respectively. These results are also

TABLE 6 Isotropic chemical shifts (σ_{iso}) and *z*-axis components (σ_{zz}) in the inflection points of the NICS scans on ring 1, 2, and 3 of NL1-NL17 dyes

	Ring 1		Ring 2		Ring 3	
Dyes	σ_{iso}	σ_{zz}	σ_{iso}	σ_{zz}	σ_{iso}	σ_{zz}
NL1	−9.87	−19.72	−1.40	−16.34	−8.19	−20.00
NL2	−9.73	−18.77	−1.45	−14.00	−8.20	−20.38
NL3	−8.67	−18.49	−0.74	−12.98	−8.13	−20.32
NL4	−8.47	−18.72	−0.53	−12.11	−8.13	−20.43
NL5	−9.95	−23.12	−11.74	−27.61	−4.48	−22.44
NL6	−4.54	−17.95	−9.10	−21.39	−4.12	−19.75
NL7	−4.35	−21.55	−9.25	−19.93	−0.80	−12.65
NL8	−2.39	−18.73	−9.25	−23.14	−1.13	−16.37
NL9	−2.42	−17.47	−8.61	−21.98	−0.87	−15.23
NL10	−4.04	−17.88	−9.07	−21.37	−4.19	−19.96
NL11	−2.91	−16.82	−8.59	−20.47	−4.49	−20.76
NL12	−3.91	−19.89	−9.96	−33.35	−1.51	−21.22
NL13	−4.42	−20.93	−10.72	−22.14	−1.28	−16.42
NL14	−2.67	−19.87	−10.77	−36.14	−1.77	−24.01
NL15	−7.20	−17.35	−8.66	−22.34	−0.95	−15.87
NL16	−5.93	−17.93	−10.12	−20.66	−1.58	−16.83
NL17	−1.36	−16.85	−9.95	−32.12	−2.14	−22.99

Notes: NICS values are given in ppm.

obtained with σ_{iso}, indicating that the aromaticity decreases in ring 2 of the NL1-NL4 dyes. σ_{iso} gives the same values and tendency for both ring 1 and ring 3.

Nevertheless, σ_{zz} NICS values shed some light on the aromaticity response of the π-bridge groups. In this sense, NL1-NL5 dyes with thiophene as the π-bridge present the highest local aromaticity in ring 3, next followed by NL6, NL9, NL12 and NL15 dyes, which have phenyl as the π-bridge, and NL8, NL11, NL14, and NL17 dyes with pyrazine, and finally, the NL7, NL10, NL13 and NL16 dyes with pyridine. These results show that the aromatic response of thiophene and pyrazine as the π-bridge is strengthened as a consequence of their similarity to thieno[3,4-b] pyrazine.

Summarizing these results, the single isotropic σ_{iso} and *z*-axis components σ_{zz} NICS values of rings 1-3 revealed two different behaviors, the first one shows that, in the NL1-NL4 dyes, rings 1 and 3 are more aromatic than rings 2, while in the, NL5-NL17 dyes, the aromaticity is stronger in ring 2. These results suggest that the pro-aromatic behavior of these dyes can be understood as the increase from ring 1 to ring 2 on the thieno [3,4-b]pyrazine. Consequently, the NL1-NL4 dyes are weakly pro-aromatic, while the NL5-NL17 dyes are strongly pro-aromatic. In this context, the highest gain in aromaticity is manifested in the NL12 dye. This highly pro-aromatic behavior can stabilize the LUMO orbital and cause the low energy gap and the redshift of the wavelength, as shown in the previous sections. Consequently, this study proposes that the NL12 dye could also present high overall efficiency in a solar cell (η).

3.3 | Structural, energetic, and electronic analysis in the adsorption of NL1, NL6-NL8, and NL15 on $(TiO_2)_{72}$: studying the *electron injection step* from the chemical viewpoint

Taking into account the results of the above section, most representatives pro-aromatic organic dyes are chosen to study the *electron injection* step. In this context, NL6 is the best sensitizer reported (PCE = 7.08%), and NL7-NL8 are the worst ones (PCE = 0.83% and 0.89%, respectively). NL1 and NL15 are potential sensitizers presenting novel chemical characteristics similar to NL6, such as an electron deficient acceptor group (A) and donor and highly aromatic π-bridge groups (thiophene and phenyl, respectively). Therefore, this study calculates the NL1@$(TiO_2)_{72}$, NL6@$(TiO_2)_{72}$, NL7@$(TiO_2)_{72}$, NL8@$(TiO_2)_{72}$, and NL15@$(TiO_2)_{72}$ systems, involving three adsorption modes. The first mode that coordinates the dye to the surface through N and O atoms, labeled as Bid_CN_COOH. The next one coordinates two, or just one, O atoms in a bidentate and monodentate adsorption mode, Bid_COO_H, and Mono_COOH, respectively. It is essential to highlight that, recently, Bid_CN_COOH has been found to be the stablest adsorption mode,[58,98] contrary to previous works which reported it to be the bidentate mode.[101] Figure 7 shows the geometrical parameters associated with NL1@$(TiO_2)_{72}$, NL6@$(TiO_2)_{72}$, NL7@$(TiO_2)_{72}$ and NL8@$(TiO_2)_{72}$ when the Bid_CN_COOH mode is studied. Figure S7 (SI) shows the parameters of these dyes when Bid_COO_H, and Mono_COOH are studied. The results show that the Ti-N and Ti-O bonds are longer in the NL7@$(TiO_2)_{72}$ and NL8@$(TiO_2)_{72}$ systems than in the NL1@$(TiO_2)_{72}$, and NL6@$(TiO_2)_{72}$ systems. This result demonstrates

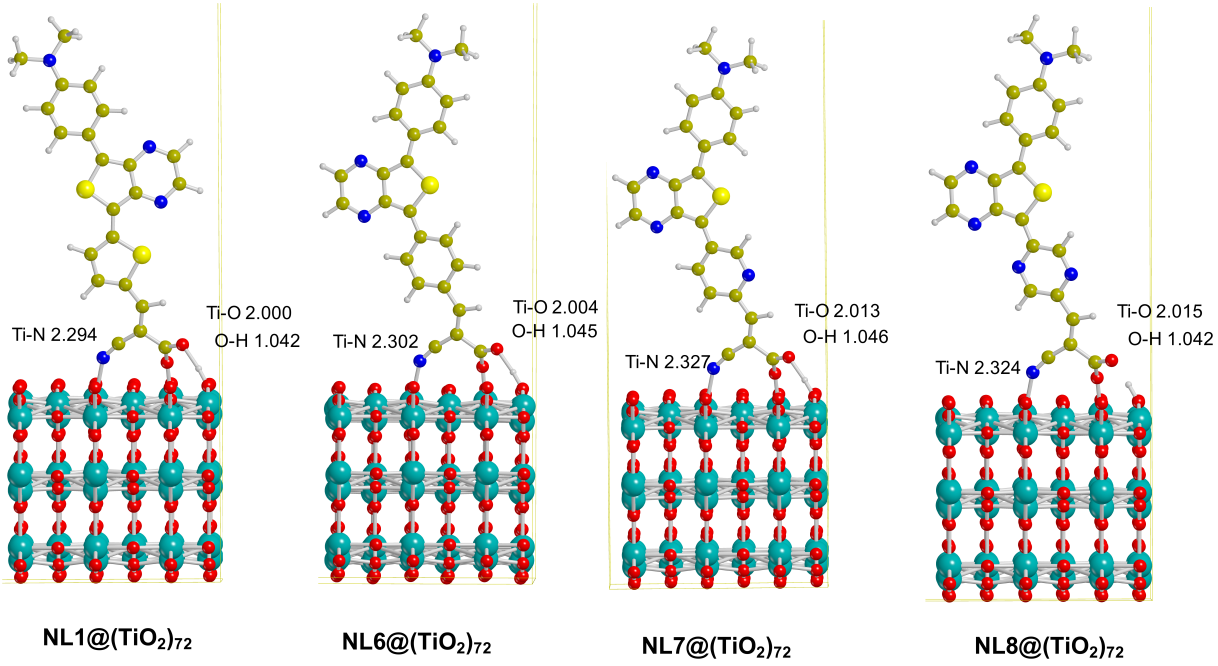

FIGURE 7 Most stable adsorption mode, Bid_CN_COOH, and geometrical parameters of NL1, NL6, NL7, and NL8 into the TiO_2 surface calculated using the PBED + U functional. All the distances are given in Angstrom (Å)

TABLE 7 Adsorption energies (ΔE_{ads} + ΔE_L) of NL1, NL6-NL8, and NL15 into $(TiO_2)_{72}$ using the PBE + D + U functional

dye@TiO_2	Bid_CN_COOH	Bid_COO_H	Mono_COOH
NL1@$(TiO_2)_{72}$	−1.54	−1.32	−1.11
NL6@$(TiO_2)_{72}$	−1.63	−1.22	−1.17
NL7@$(TiO_2)_{72}$	−1.62	−1.18	−1.18
NL8@$(TiO_2)_{72}$	−1.59	−1.19	−1.09
NL15@$(TiO_2)_{72}$	—	−1.35	−1.37

Notes: Values are in eV.

the low efficiency of the latter, because a long bond distance between the atoms of the anchoring group and the TiO_2 surface does not allow an adequate electron transfer because of the low overlap between the electron density of the atoms.

Furthermore, the adsorption energies with correction for the lateral interactions (ΔE_{ads} + ΔE_L) of the NL1@$(TiO_2)_{72}$, NL6@$(TiO_2)_{72}$, NL7@$(TiO_2)_{72}$, NL8@$(TiO_2)_{72}$, and NL15@$(TiO_2)_{72}$ systems are studied using the Equation 1 and 2. The results are tabulated in Table 7 and show that in the NL1@$(TiO_2)_{72}$, NL6@$(TiO_2)_{72}$, NL7@$(TiO_2)_{72}$, and NL8@$(TiO_2)_{72}$ systems, the Bid_CN_COOH coordination mode is the most stable, with values between −1.54 and −1.63 eV, while in the NL15@$(TiO_2)_{72}$ with RCOOH as anchoring group, the Bid_COO_H coordination mode is the most stable. These results are similar to those reported for other metal-free organic dyes.[58] It is essential to observe that the energy difference between the Bid_CN_COOH mode and the next stablest modes (Bid_COO_H or Mono_COOH) is 0.22 to 0.50 eV, while the energy difference between Bid_COO_H and Mono_COOH is 0.00 to 0.22 eV. These slight differences could suggest the presence of more than one coordination mode in the solar cell surface, as proposed recently.[111] Moreover, it is important to mention that the adsorption energies of Bid_CN_COOH are very close. These present only a difference energy of 0.08 eV between the most stable, the NL6@$(TiO_2)_{72}$ system and, the lowest one, the NL1@$(TiO_2)_{72}$. Therefore, these results cannot explain the highest efficiency of the NL6 neither lowest to NL7 and NL8. In this sense, the adsorption energies of pro-aromatic organic dyes to the TiO_2 surface does not depend only on the electronic characteristics of the anchoring-TiO_2 bonds.

To continue scrutinizing the adsorption of pro-aromatic organic dyes onto TiO_2, the electronic density of states (DOS) is examined. The results are described in Figure 8 and Figure S8 of the SI. In a sense, the band gaps of NL1@$(TiO_2)_{72}$, NL6@$(TiO_2)_{72}$, NL7@$(TiO_2)_{72}$, NL8@$(TiO_2)_{72}$ and NL15@$(TiO_2)_{72}$ were obtained between 3.2 and 3.3 eV, which shows that the gap energies are not determinant in the *electron injection* step. These similar results are due to the comparable density of states obtained. Specifically, the valence band edge is generally dominated by O (2 seconds, 2p), followed by Ti (2p), and in low contribution, the elements C, H, N and S of the dyes, while the conduction band edge is completely formed by Ti (3d). This behavior ensures the electron movement and leads to the hole-electron formation in the valence band in the dye@TiO_2 interaction. Nevertheless, the main differences are found when the frontier orbitals HOMO and LUMO are inspected (See Figure 8). In the NL1@

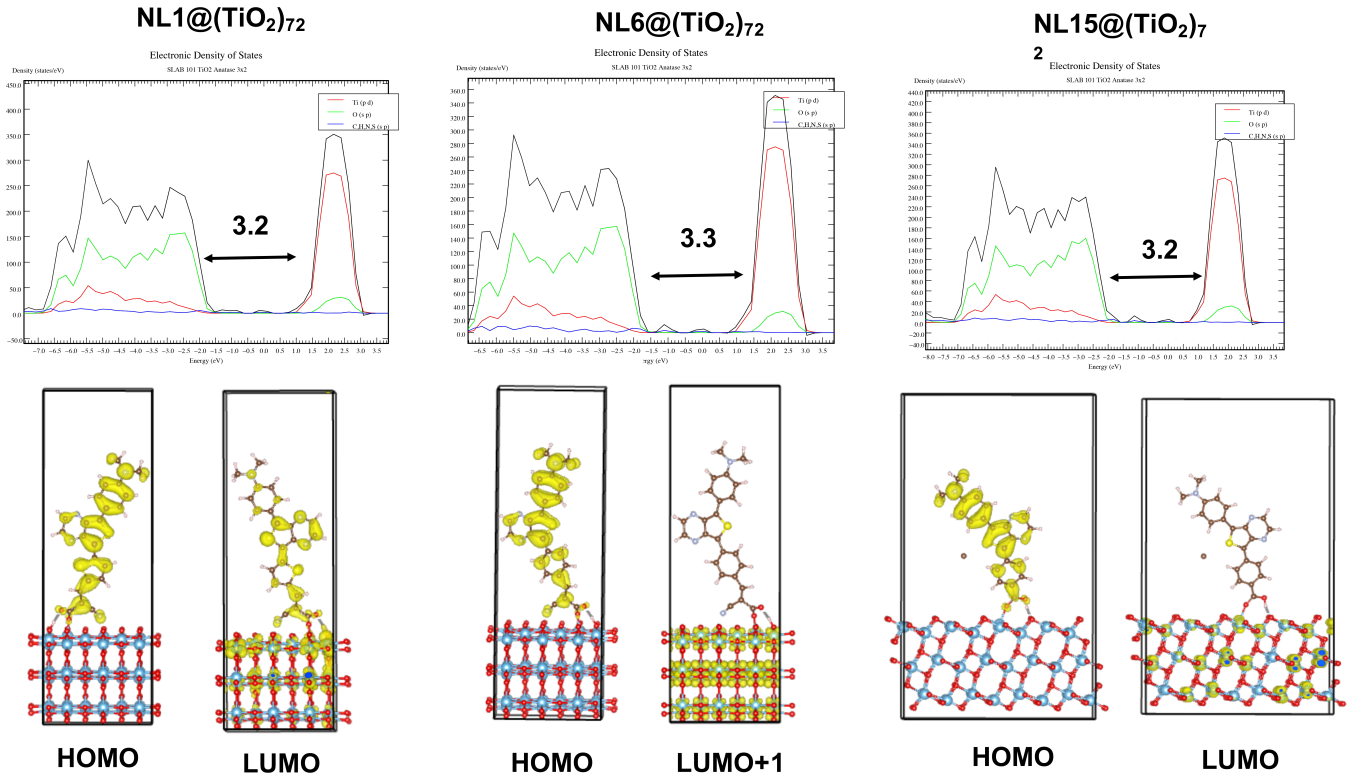

FIGURE 8 DOS graphics and plot of the first HOMO and LUMO orbitals to NL1@$(TiO_2)_{72}$, NL6@$(TiO_2)_{72}$, and NL15@$(TiO_2)_{72}$ systems. DOS graphics show the total density in black, while the partial DOS for the Ti(p,d) and O(p) are in red and green, respectively. DOS, density of states

TABLE 8 Free energies change for the electron injection (ΔG_{inject}) and its contributions (ΔG_{redox}) and (ΔG_{ads})

dye@TiO_2	ΔG_{inject}	ΔG_{redox}	ΔG_{ads}
NL1@$(TiO_2)_{72}$	−2.32	−1.96	−0.36
NL6@$(TiO_2)_{72}$	−2.38	−1.98	−0.40
NL7@$(TiO_2)_{72}$	−2.36	−1.93	−0.43
NL8@$(TiO_2)_{72}$	−2.41	−1.94	−0.47
NL15@$(TiO_2)_{72}$	−1.72	−0.77	−0.95

Notes: Values are in eV.

$(TiO_2)_{72}$, NL6@$(TiO_2)_{72}$, and NL15@$(TiO_2)_{72}$ systems, the electron densities of the HOMOs are in all the dye structures and the electron densities of the LUMOs are located on the Ti atoms. In the NL7@$(TiO_2)_{72}$ and NL8@$(TiO_2)_{72}$ systems, the HOMOs and LUMOs present electron densities wholly located on the dyes (Figure S8). These results confirm that the low overall power conversion efficiency (η) in the pro-aromatic organic dyes NL7 and NL8 is also generated because the electron densities of the LUMOs are not located on the Ti atoms of the TiO_2 surface, preventing that the electron from moving quickly to the conduction band and avoiding the next step in the solar cell, which is the redox reaction. Conversely, NL1 and NL15 are confirmed as potential dyes, because similar to NL6, (the pro-aromatic organic dye with the highest efficiency), the LUMOs present electronic densities over the Ti atoms of the surface, allowing fast *electron injection* to the conduction band of the TiO_2 surface.

We have complemented the above results with the adsorption free energies (ΔG_{ads}) in the Bid_CN_COOH coordination modes of the dyes@TiO_2 systems using the Equation (1). The values are tabulated in Table 8, where the adsorption free energies are also very close. Nevertheless, an opposite effect to that expected is obtained: NL6, the most efficient sensitizer, is not very spontaneous in the adsorption TiO_2. Consequently, the free energies change for the electron injection (ΔG_{inject}) was analyzed using the Equation (3), and the redox free energy (ΔG_{redox}) is found as an energetic contribution. For the former, close values between −2.32 and 2.41 eV are found, which suggests as in ΔG_{ads} that the global energies of the process do not describe the experimental results. However, the redox free energies (ΔG_{redox}) reproduce the experimental tendencies: NL6@$(TiO_2)_{72}$ system present the highest contribution, while NL7@$(TiO_2)_{72}$ and NL8@$(TiO_2)_{72}$, the lowest one. These outstanding results indicate that if pro-aromatic organic dyes are employed in DSSC, the *electron injection* step will present a more significant contribution to the redox reaction (dye* → $dye^+ + e^-$) than to the adsorption stage ($dye^+ + TiO_2$ → dye@TiO_2).

Therefore, the specific aromatic behavior of these dyes affects the electron injection in a manner that has not been explained for other traditional D-A-π-A dyes, because in these dyes type the redox reaction is the key process into this step.

3.4 | The *electron injection step* into the L1@$(TiO_2)_{72}$, SGT-130@$(TiO_2)_{72}$ and PB1@$(TiO_2)_{72}$ systems: a comparative analysis of the role of the acceptor group A, in D-A-π-A type dyes

Aiming to analyze the role of the acceptor group A in D-A-π-A type dyes, the sensitizers L1, SGT-130 and PB1 were studied in the *electron injection* step of the solar cell. In these dyes, a small donor group D is used to reduce the steric effect of the dye@$(TiO_2)_{72}$. The geometrical parameters of the L1@$(TiO_2)_{72}$, SGT-130@$(TiO_2)_{72}$, and PB1@$(TiO_2)_{72}$ systems are described in Figure 9 and Figure S9 (SI). The first shows the Bid_CN_COOH adsorption mode, and the second, the Bid_COO_H, and Mono_COOH modes. The results show structures analogous to NL1-NL17@$(TiO_2)_{72}$, as previously found. The Ti-N and Ti-O bond lengths are about 2.280 and 2.000 Å, respectively. Furthermore, the adsorption energies calculated using the Equation (1) and tabulated in Table 9 show that Bid_CN_COOH is the stablest coordination mode. The lowest adsorption energy is obtained in SGT-130@$(TiO_2)_{72}$, which is contrary to the high efficiency reported for this metal-free organic dye. Moreover, when the density of states (DOS) is explored and the electronic density is analyzed in the frontier HOMO and LUMO orbitals of the dye@$(TiO_2)_{72}$ systems (Figure 10), the electron injection is possible because of the Ti(3d) atoms that contribute to the conduction bands. However, it is only efficient in SGT-130@$(TiO_2)_{72}$. This behavior is attributed to the differences in electronic density over the LUMO found in L1@$(TiO_2)_{72}$, SGT-130@$(TiO_2)_{72}$, and PB1@$(TiO_2)_{72}$. Specifically, L1@$(TiO_2)_{72}$ and PB1@$(TiO_2)_{72}$ present the electronic density of the LUMO over the entire dye structure, while this is located over the Ti atoms of the SGT-130@$(TiO_2)_{72}$ system, which facilitate electron movement.

The overall process is studied using the free energies change for the electron injection (ΔG_{inject}) (Equation 3.) Also, the redox (ΔG_{redox}) and adsorption (ΔG_{ads}) free energies are obtained. The values are tabulated in Table 10 and show that the highest electron injection and redox contribution was obtained for the SGT-130@$(TiO_2)_{72}$ system, which agrees with the experimental results of the overall power conversion efficiency (η = 10.1%). Therefore, the highest electron injection of the SGT-130 dye results from the most spontaneous process (dye* → $dye^+ + e^-$). Finally, a comparison is made between the redox free energies of NL1@$(TiO_2)_{72}$, PB1@$(TiO_2)_{72}$, and SGT-130@$(TiO_2)_{72}$, which have thieno[3,4-*b*]pyrazine

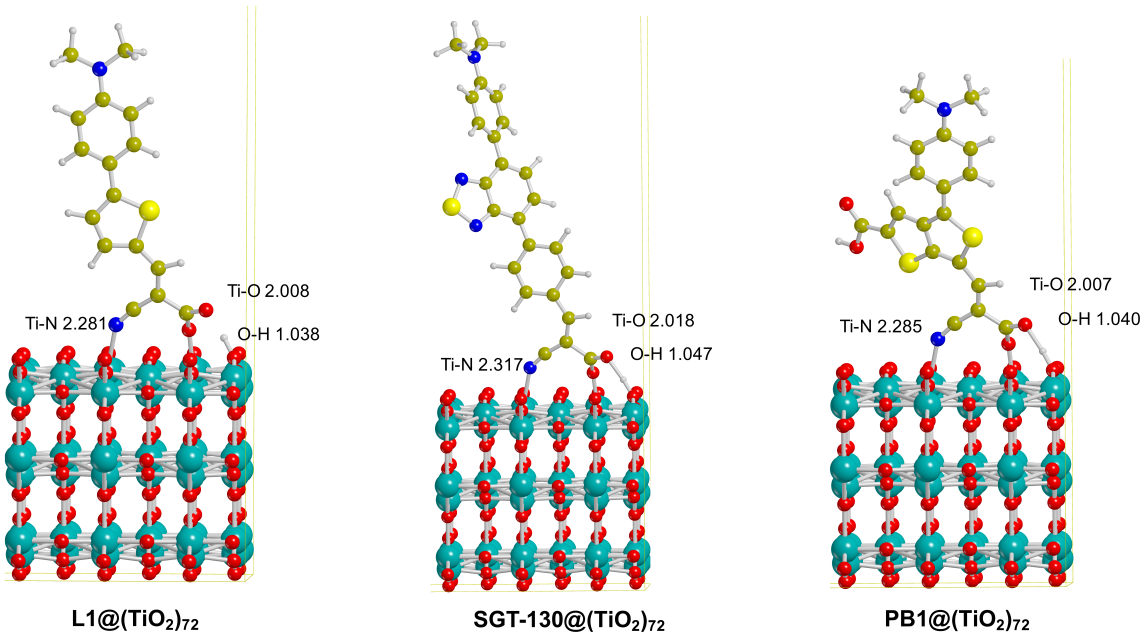

FIGURE 9 Stablest adsorption mode, Bid_CN_COOH, and geometrical parameters of L1, SGT-130, PB1 into the TiO_2 surface calculated using the PBED + U + D functional. All the distances are given in Ångström (Å)

TABLE 9 Adsorption energies (ΔE_{ads} + ΔE_L) of some important dyes into $(TiO_2)_{72}$ using the PBE + D + U functional

dye@TiO_2	Bid_CN_COOH	Bid_COO_H	Mono_COOH
L1@$(TiO_2)_{72}$	−1.62	−1.28	−1.28
SGT-130@$(TiO_2)_{72}$	−1.55	−1.30	−1.22
PB1@$(TiO_2)_{72}$	−1.73	−1.22	−1.14

Notes: Values are in eV.

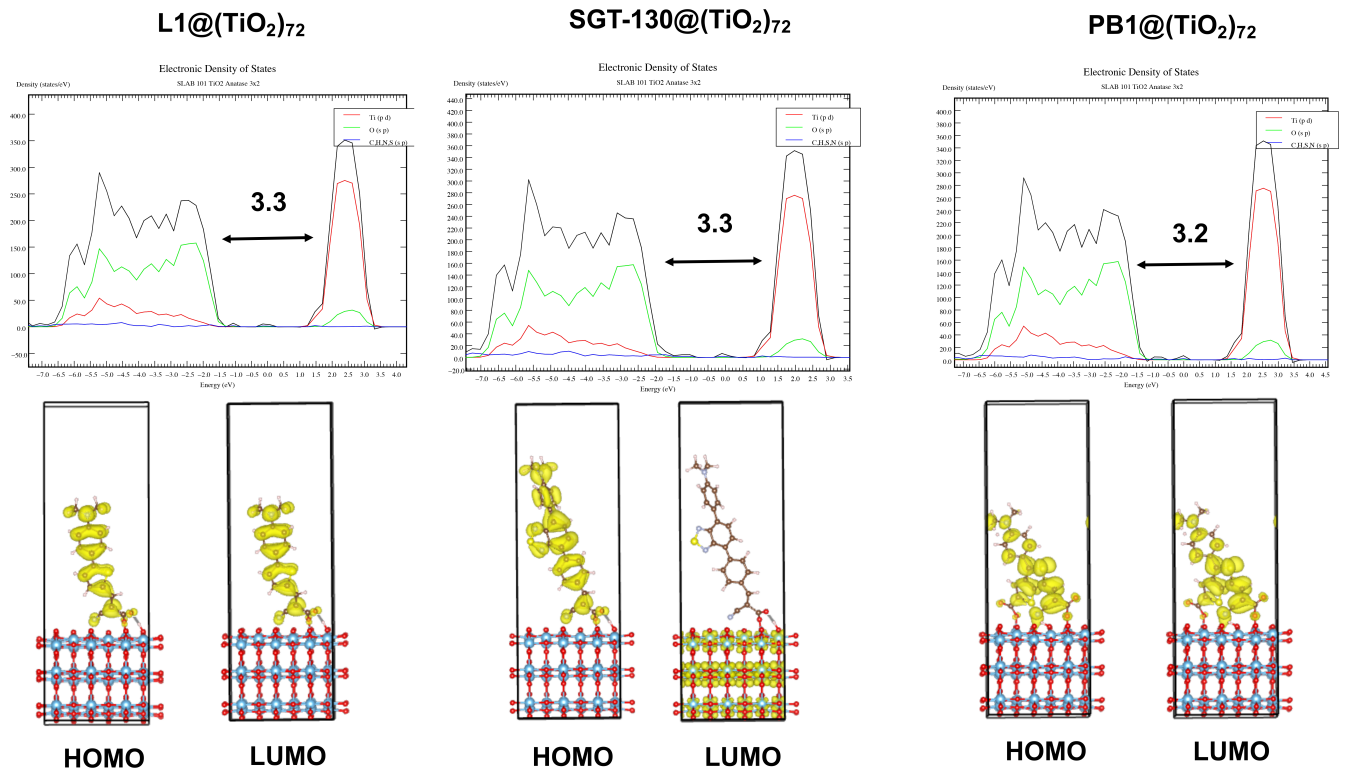

FIGURE 10 DOS graphics and plot of the first HOMO and LUMO orbitals for L1@$(TiO_2)_{72}$, SGT-130@$(TiO_2)_{72}$, and PB1@$(TiO_2)_{72}$. DOS graphics show the total density in black, while the partial DOS for the Ti(p,d) and O(p) are in red and green, respectively. DOS, density of states

dye@TiO_2	ΔG_{inject}	ΔG_{redox}	ΔG_{ads}
L1@$(TiO_2)_{72}$	−1.82	−1.39	−0.43
SGT-130@$(TiO_2)_{72}$	−2.14	−1.77	−0.37
PB1@$(TiO_2)_{72}$	−2.03	−1.41	−0.62

Notes: Values are in eV.

TABLE 10 Free energies change for the electron injection (ΔG_{inject}) and its contributions (ΔG_{redox}) and (ΔG_{ads})

(Tpy), thieno[3,4-*b*]thiophene (TTh), and benzothiadiazole (BTD), as acceptor groups, A, respectively. L1@$(TiO_2)_{72}$, had the simplest D-π-A. The results show that the addition of thieno[3,4-*b*]thiophene does not produce significant changes. Nevertheless, if the benzothiadiazole or thieno [3,4-*b*]pyrazine (Tpy) are used, more spontaneous processes are obtained. Therefore, the structural design of novel sensitizers can be focused on dyes like NL1, NL6, and SGT-130.

4 | CONCLUSIONS

The most efficient and the most potential sensitizers, NL6 and NL12, respectively, present a D-A-π-A rearrangement in which, the 2,3-di-TPz (A) is a weak acceptor, the π-bridge is electron rich, and the anchoring group (A) is highly electron accepting. Therefore, the chemical nature of the D-A-π-A dye favors the highest behavior as photosensitizer.

Some sensitizers such as NL1, NL6, NL10, and NL12 show bands extended to the infrared region (>550 nm), which could be the reason for the highest performance in the photoexcitation step. Moreover, dyes with donors π-bridge, such as, NL7 and NL8, are the most inefficient, because the inner orbitals (H-8, H-6) control the electronic transitions in the visible region.

The pro-aromatic behavior of these dyes can be understood as gaining aromaticity from the thiophene group to the pyrazine ring on thieno [3,4-b]pyrazine. This demonstrates that in the metal-free sensitized type D-A-π-A the acceptor group determines many of the properties of the molecule.

In the sensitizers of the NLX family, the electron injection stage does not depend solely on the electronic characteristics of the anchoring-TiO_2 bonds. This stage is strongly driven by the redox energy contribution and the pro-aromatic behavior of the dye.

Benzothiadiazole (BTD) and thieno[3,4-*b*]pyrazine (Tpy) are outstanding acceptor groups A. These are ideal substituents in the structural design of novel D-A-π-A sensitizers due to their high electron injection performance.

ACKNOWLEDGMENTS

K.P-G. specially acknowledges FONDECYT for projects 3170117. F.M, D.P-H and R.A-P acknowledge to FONDECYT for projects 1180158, 1140503, and 1150629, respectively. Moreover, this work was funded by CONICYT AKA ERNC-001 project and RC120001 project of the Iniciativa Científica Milenio (ICM) del Ministerio de Economía, Fomento y Turismo del Gobierno de Chile. Finally, K.P-G. acknowledges "CONICYT +PAI+CONVOCATORIA NACIONAL SUBVENCIÓN A INSTALACIÓN EN LA ACADEMIA CONVOCATORIA AÑO 2018 + PAI77180024."

ORCID

Katherine Paredes-Gil https://orcid.org/0000-0002-1407-8752
Dayán Páez-Hernández https://orcid.org/0000-0003-2747-9982
Ramiro Arratia-Pérez https://orcid.org/0000-0001-6140-2116
Fernando Mendizábal https://orcid.org/0000-0002-6912-8630

REFERENCES

[1] A. Hagfeldt, G. Boschloo, L. Sun, L. Kloo, H. Pettersson, *Chem. Rev.* **2010**, *110*, 6595.
[2] M. Pastore, T. Etienne, F. De Angelis, *J. Mater. Chem. C* **2016**, *4*, 4346.
[3] A. Carella, F. Borbone, R. Centore, *Front. Chem.* **2018**, *6*, 1.
[4] X. Wang, Z. M. Wang, *High-efficiency Solar Cells*, Springer, Berlin Heidelberg **2014**.
[5] M. A. Green, Y. Hishikawa, E. D. Dunlop, D. H. Levi, J. Hohl-Ebinger, M. Yoshita, A. W. Y. Ho-Baillie, *Prog. Photovoltaics Res. Appl.* **2019**, *27*, 3.
[6] J. Schneider, M. Matsuoka, M. Takeuchi, J. Zhang, Y. Horiuchi, M. Anpo, D. W. Bahnemann, *Chem. Rev.* **2014**, *114*, 9919.
[7] S. Banerjee, S. C. Pillai, P. Falaras, K. E. O'Shea, J. A. Byrne, D. D. Dionysiou, *J. Phys. Chem. Lett.* **2014**, *5*, 2543.
[8] B. O'Regan, M. Grätzel, *Nature* **1991**, *353*, 737.
[9] M. K. Nazeeruddin, A. Kay, E. Miiller, P. Liska, N. Vlachopoulos, M. Grätzel, *J. Am. Chem. Soc.* **1993**, *115*, 6382.
[10] Y. Jo, C. Jung, J. Lim, B. H. Kim, C.-H. Han, J. Kim, S. Kim, D. Kim, Y. Jun, *Electrochim. Acta* **2012**, *66*, 121.
[11] T. Bessho, E. Yoneda, J. Yum, M. Guglielmi, I. Tavernelli, H. Imai, U. Rothlisberger, M. K. Nazeeruddin, M. Grätzel, *J. Am. Chem. Soc.* **2009**, *131*, 5930.
[12] L.-L. Li, E. W.-G. Diau, *Chem. Soc. Rev.* **2013**, *42*, 291.
[13] R. Urzúa-Leiva, R. Pino-Rios, G. Cárdenas-Jirón, *Phys. Chem. Chem. Phys.* **2019**, *21*, 4339.
[14] T. Bessho, S. M. Zakeeruddin, C. Yeh, E. W. Diau, M. Grätzel, *Angew. Chem. Int. Ed. Engl.* **2010**, *49*, 6646.
[15] A. Yella, H.-W. Lee, H. N. Tsao, C. Yi, A. K. Chandiran, M. K. Nazeeruddin, E. W.-G. Diau, C.-Y. Yeh, S. M. Zakeeruddin, M. Grätzel, *Science* **2011**, *334*, 629.
[16] S. Mathew, A. Yella, P. Gao, R. Humphry-Baker, B. F. E. Curchod, N. Ashari-Astani, I. Tavernelli, U. Rothlisberger, M. K. Nazeeruddin, M. Grätzel, *Nat. Chem.* **2014**, *6*, 242.
[17] S. Shafian, J. Son, Y. Kim, J. K. Hyun, K. Kim, *ACS Appl. Mater. Interfaces* **2019**, *11*, 18887.
[18] J. Liu, B. Liu, Y. Tang, W. Zhang, W. Wu, Y. Xie, W.-H. Zhu, J. Mater, *Chem. C* **2015**, *3*, 11144.
[19] K. Kakiage, Y. Aoyama, T. Yano, T. Otsuka, T. Kyomen, M. Unno, M. Hanaya, *Chem. Commun. (Camb).* **2014**, *50*, 6379.
[20] K. Kakiage, Y. Aoyama, T. Yano, K. Oya, J. Fujisawa, M. Hanaya, *Chem. Commun.* **2015**, *51*, 15894.
[21] J. B. Yang, P. Ganesan, J. Teuscher, T. Moehl, Y. J. Kim, C. Y. Yi, P. Comte, K. Pei, T. W. Holcombe, M. K. Nazeeruddin, J. L. Hua, S. M. Zakeeruddin, H. Tian, M. Grätzel, *J. Am. Chem. Soc.* **2014**, *136*, 5722.
[22] J. H. Delcamp, A. Yella, M. K. Nazeeruddin, M. Grätzel, *Chem. Commun. (Camb).* **2012**, *48*, 2295.
[23] M. K. R. Fischer, S. Wenger, M. Wang, A. Mishra, S. M. Zakeeruddin, M. Grätzel, P. Bäuerle, *Chem. Mater.* **2010**, *22*, 1836.
[24] C. M. Ip, A. Troisi, *J. Phys. Chem. Lett.* **2016**, *7*, 2989.
[25] J. Luo, M. Xu, R. Li, K. Huang, C. Jiang, Q. Qi, W. Zeng, J. Zhang, C. Chi, P. Wang, J. Wu, *J. Am. Chem. Soc.* **2014**, *136*, 265.
[26] W. Li, Z. Liu, H. Wu, Y.-B. Cheng, Z. Zhao, H. He, *J. Phys. Chem. C* **2015**, *119*, 5265.
[27] W. Zhu, Y. Wu, S. Wang, W. Li, X. Li, J. Chen, Z. S. Wang, H. Tian, *Adv. Funct. Mater.* **2011**, *21*, 756.
[28] Y. Wu, W. Zhu, *Chem. Soc. Rev.* **2013**, *42*, 2039.
[29] Y. Wu, W. H. Zhu, S. M. Zakeeruddin, M. Grätzel, *ACS Appl. Mater. Interfaces* **2015**, *7*, 9307.
[30] Y. K. Eom, I. T. Choi, S. H. Kang, J. Lee, J. Kim, M. J. Ju, H. K. Kim, *Adv. Energy Mater.* **2015**, *5*, 1.
[31] D. Joly, L. Pelleja, S. Narbey, O. Frederic, C. Julien, J. N. Clifford, E. Palomares, R. Demadrille, *Sci. Rep.* **2014**, *4*, 4033.
[32] D. Joly, L. Pelleja, S. Narbey, F. Oswald, T. Meyer, Y. Kervella, P. Maldivi, J. N. Clifford, E. Palomares, R. Demadrille, *Energy Environ. Sci.* **2015**, *8*, 2010.
[33] X. Kang, J. Zhang, D. O. Neil, A. J. Rojas, W. Chen, P. Szymanski, S. R. Marder, M. A. El-Sayed, *Chem. Mater.* **2014**, *26*, 4486.
[34] W. Li, Y. Wu, Q. Zhang, H. Tian, W. Zhu, *ACS Appl. Mater. Interfaces* **2012**, *4*, 1822.
[35] Y. Wu, M. Marszalek, S. M. Zakeeruddin, Q. Zhang, H. Tian, M. Grätzel, W. Zhu, *Energy Environ. Sci.* **2012**, *5*, 8261.
[36] P. Liu, W. Sharmoukh, B. Xu, Y. Y. Li, G. Boschloo, L. Sun, L. Kloo, *ACS Omega* **2017**, *2*, 1812.
[37] M. Katono, M. Wielopolski, M. Marszalek, T. Bessho, J. Moser, R. Humphry-baker, S. M. Zakeeruddin, M. Gra, *J. Phys. Chem. C* **2014**, *118*, 16486.

[38] F. Lu, S. Qi, J. Zhang, G. Yang, B. Zhang, Y. Feng, *Dye. Pigment.* **2017**, *141*, 161.
[39] Z. Liu, K. Duan, H. Guo, Y. Deng, H. Huang, X. Yi, H. Chen, S. Tan, *Dye. Pigment.* **2017**, *140*, 312.
[40] M. Grishina, O. Bol'shakov, A. Potemkin, V. Potemkin, *Dye. Pigment.* **2017**, *144*, 80.
[41] Y. Wang, Z. Zheng, T. Li, N. Robertson, H. Xiang, W. Wu, J. Hua, W. H. Zhu, H. Tian, *ACS Appl. Mater. Interfaces* **2016**, *8*, 31016.
[42] Q. Huang, L. Guo, N. Wang, X. Zhu, S. Jin, B. Tan, *ACS Appl. Mater. Interfaces* **2019**, *11*, 15861.
[43] P. Brogdon, F. Giordano, G. A. Puneky, A. Dass, S. M. Zakeeruddin, M. K. Nazeeruddin, M. Grätzel, G. S. Tschumper, J. H. Delcamp, *Chem. - A Eur. J.* **2016**, *22*, 694.
[44] N. P. Liyanage, A. Yella, M. Nazeeruddin, M. Grätzel, J. H. Delcamp, *ACS Appl. Mater. Interfaces* **2016**, *8*, 5376.
[45] X. Lu, G. Zhou, H. Wang, Q. Feng, Z.-S. Wang, *Phys. Chem. Chem. Phys.* **2012**, *14*, 4802.
[46] Z. Zeng, X. Shi, C. Chi, J. T. López Navarrete, J. Casado, J. Wu, *Chem. Soc. Rev.* **2015**, *44*, 6578.
[47] M. Pastore, A. Selloni, S. Fantacci, F. De Angelis, in *First Principles Approaches to Spectroscopic Properties of Complex Materials* (Eds: C. Di Valentin, S. Botti, M. Cococcioni), Springer, Berlin Heidelberg **2014**, p. 1.
[48] S. Fantacci, F. De Angelis, *Eur. J. Inorg. Chem.* **2019**, *2019*, 743.
[49] S. Grimme, P. R. Schreiner, *Angew. Chemie Int. Ed.* **2018**, *57*, 4170.
[50] F. De Angelis, S. Fantacci, E. Mosconi, M. K. Nazeeruddin, M. Grätzel, *J. Phys. Chem. C* **2011**, *115*, 8825.
[51] Y. F. Liu, J. Guan, D. Hu, L. Du, H. Sun, J. Gao, J. Zhao, Z. Lan, J. Phys, *Chem. C* **2015**, *119*, 8417.
[52] X. Zarate, E. Schott, T. Gomez, R. Arratia-Pérez, J. Phys, *Chem. A* **2013**, *117*, 430.
[53] T. Le Bahers, T. Pauporté, P. P. Lainé, F. Labat, C. Adamo, I. Ciofini, *J. Phys. Chem. Lett.* **2013**, *4*, 1044.
[54] F. Mendizabal, A. Lopéz, R. Arratia-Pérez, G. Zapata-Torres, *Comput. Theor. Chem.* **2015**, *1070*, 117.
[55] F. Mendizabal, A. Lopéz, R. Arratia-Pérez, N. Inostroza, C. Linares-Flores, *J. Mol. Model.* **2015**, *21*, 226.
[56] Z. L. Cai, M. J. Crossley, J. R. Reimers, R. Kobayashi, R. D. Amos, *J. Phys. Chem. B* **2006**, *110*, 15624.
[57] S. Ikäläinen, K. Laasonen, *Phys. Chem. Chem. Phys.* **2013**, *15*, 11673.
[58] W. C. Chen, S. Nachimuthu, J. C. Jiang, *Sci. Rep.* **2017**, *7*, 1.
[59] J. K. Roy, S. Kar, J. Leszczynski, *Sci. Rep.* **2018**, *8*, 1.
[60] T. Gomez, F. Jaramillo, E. Schott, R. Arratia-Pérez, X. Zarate, *Sol. Energy* **2017**, *142*, 215.
[61] Z. Hu, H. Metiu, *J. Phys. Chem. C* **2011**, *115*, 5841.
[62] S. Tosoni, O. Lamiel-Garcia, D. Fernandez Hevia, J. M. Doña, F. Illas, *J. Phys. Chem. C* **2012**, *116*, 12738.
[63] E. German, R. Faccio, A. W. Mombrú, *Appl. Surf. Sci.* **2018**, *428*, 118.
[64] Q. Zhao, H. J. Kulik, *J. Chem. Theory Comput.* **2018**, *14*, 670.
[65] R. Parr, W. Yang, *Density functional theory of atoms and molecules.* Editorial: Oxford University Press, New York, Oxford. 1989. p.IX + 333 pp. molecules **1989**.
[66] G. E, M. J. Frisch, G. W. Trucks, H. B. Schlegel, V. Scuseria, M. Robb, M. A, J. R. Cheeseman, G. Scalmani, H. B. Barone, G. A. Petersson, H. Nakatsuji, M. Caricato, X. Li, M. Hratchian, A. F. Izmaylov, J. Bloino, G. Zheng, J. L. Sonnenberg, M. Hada, N. Ehara, K. Toyota, R. Fukuda, J. Hasegawa, J. Ishida, Y. Honda, O. Kitao, H. Nakai, T. Vreven, J. A. Montgomery, K. Peralta, J. E, F. Ogliaro, M. Bearpark, J. J. Heyd, K. Brothers, K. N, V. N. Staroverov, R. Kobayashi, J. Normand, M. Raghavachari, R. Rendell, J. C. Burant, S. S. Iyengar, J. Tomasi, V. Cossi, N. J. Millam, M. Klene, J. E. Knox, J. B. Cross, O. Bakken, C. Adamo, J. Jaramillo, R. Gomperts, R. E. Stratmann, R. L. Yazyev, A. J. Austin, R. Cammi, C. Pomelli, J. W. Ochterski, P. Martin, K. Morokuma, V. G. Zakrzewski, G. A. Voth, O. Salvador, J. J. Dannenberg, S. Dapprich, A. D. Daniels, D. J. Farkas, J. B. Foresman, J. V. Ortiz, J. Cioslowski, D. J. Fox, *Gaussian09*, *Revision C.01*, Gaussian, Wallingford, CT **2016**.
[67] S. Grimme, J. Antony, S. Ehrlich, H. Krieg, *J. Chem. Phys.* **2010**, *132*, 154104.
[68] S. Grimme, *J. Comput. Chem.* **2004**, *25*, 1463.
[69] W. J. Hehre, R. Ditchfield, J. A. Pople, *J. Chem. Phys.* **1972**, *56*, 2257.
[70] A. V. Marenich, C. J. Cramer, D. G. Truhlar, *J. Phys. Chem. B* **2009**, *113*, 6378.
[71] F. Weinhold, C. R. Landies, *Discovering Chemistry With Natural Bond Orbitals* John Wiley & Sons, Inc., Hoboken, New Jersey **2012**.
[72] E. Runge, E. K. U. Gross, *Phys. Rev. Lett.* **1984**, *52*, 997.
[73] A. D. Becke, *J. Chem. Phys.* **1993**, *98*, 5648.
[74] T. Yanai, D. P. Tew, N. C. Handy, *Chem. Phys. Lett.* **2004**, *393*, 51.
[75] K. Okuno, Y. Shigeta, R. Kishi, H. Miyasaka, M. Nakano, J. Photochem, *Photobiol. A Chem.* **2012**, *235*, 29.
[76] Y. Zhao, D. G. Truhlar, *Theor. Chem. Acc.* **2007**, *120*, 215.
[77] P. V. R. Schleyer, C. Maerker, A. Dransfeld, H. Jiao, N. J. R. Van Eikema Hommes, *J. Am. Chem. Soc.* **1996**, *118*, 6317.
[78] G. te Velde, F. M. Bickelhaupt, E. J. Baerends, C. Fonseca Guerra, S. J. A. van Gisbergen, J. G. Snijders, T. Ziegler, *J. Comput. Chem.* **2001**, *22*, 931.
[79] D. Páez-Hernández, J. A. Murillo-López, R. Arratia-Pérez, *J. Phys. Chem. A* **2011**, *115*, 8997.
[80] D. Páez-Hernández, R. Arratia-Pérez, *J. Phys. Chem. A* **2012**, *116*, 7583.
[81] A. M. Lee, N. C. Handy, S. M. Colwell, *J. Chem. Phys.* **1995**, *103*, 10095.
[82] J. P. Perdew, *Phys. Rev. B* **1986**, *33*, 8822.
[83] G. Schreckenbach, *J. Chem. Phys.* **1999**, *110*, 11936.
[84] T. Helgaker, M. Jaszunski, K. Ruud, *Chem. Rev.* **1999**, *99*, 293.
[85] J. Slater, *Phys. Rev.* **1930**, *36*, 57.
[86] A. Stanger, *J. Org. Chem.* **2006**, *71*, 883.
[87] G. Kresse, J. Furthmüller, *Comput. Mater. Sci.* **1996**, *6*, 15.
[88] G. Kresse, J. Furthmüller, *Phys. Rev. B - Condens. Matter Mater. Phys.* **1996**, *54*, 11169.
[89] G. Kresse, J. Hafner, *Phys. Rev. B* **1993**, *47*, 558.
[90] J. P. Perdew, K. Burke, M. Ernzerhof, *Phys. Rev. Lett.* **1996**, *77*, 3865.
[91] V. N. Staroverov, G. E. Scuseria, J. Tao, J. P. Perdew, *Phys. Rev. B - Condens. Matter Mater. Phys.* **2004**, *69*, 1.
[92] J. Hubbard, *Proc. R. Soc. A Math. Phys. Eng. Sci.* **1963**, *276*, 238.
[93] V. I. Anisimov, I. V. Solovyev, M. A. Korotin, M. T. Czyyk, G. A. Sawatzky, *Phys. Rev. B* **1993**, *48*, 16929.

[94] M. E. Arroyo-De Dompablo, A. Morales-Garca, M. Taravillo, *J. Chem. Phys.* **2011**, *135*, 054503.
[95] T. Gomez, X. Zarate, E. Schott, R. Arratia-Perez, *RSC Adv.* **2014**, *4*, 9639.
[96] G. Kresse, J. Hafner, *J. Phys. Condens. Matter* **1994**, *6*, 8245.
[97] D. Vanderbilt, *Phys. Rev. B* **1990**, *41*, 7892.
[98] J. Feng, Y. Jiao, W. Ma, M. K. Nazeeruddin, M. Grätzel, S. Meng, *J. Phys. Chem. C* **2013**, *117*, 3772.
[99] H.-H. G. Tsai, J.-C. Hu, C.-J. Tan, Y.-C. Sheng, C.-C. Chiu, *J. Phys. Chem. A* **2016**, *120*, 8813.
[100] M. Pastore, F. De Angelis, *Phys. Chem. Chem. Phys.* **2012**, *14*, 920.
[101] C. Anselmi, E. Mosconi, M. Pastore, E. Ronca, F. De Angelis, *Phys. Chem. Chem. Phys.* **2012**, *14*, 15963.
[102] S. Pantaleone, A. Rimola, M. Sodupe, *J. Phys. Chem. C* **2017**, *121*, 14156.
[103] S. Grimme, *Chem. - A Eur. J.* **2012**, *18*, 9955.
[104] P. Mignon, P. Ugliengo, M. Sodupe, *J.Phys.chem.C* **2009**, *113*, 13741.
[105] J. H. Montoya, K. A. Persson, *Mater.* **2017**, *3*, 1.
[106] D. Mahlberg, S. Sakong, K. Forster-Tonigold, A. Groß, *J. Chem. Theory Comput.* **2019**, *15*, 3250.
[107] D. Matthews, P. Infelta, M. Grätzel, *Sol. Energy Mater. Sol. Cells* **1996**, *44*, 119.
[108] R. Katoh, A. Furube, T. Yoshihara, K. Hara, G. Fujihashi, S. Takano, S. Murata, H. Arakawa, M. Tachiya, *J. Phys. Chem.* **2004**, *108*, 4818.
[109] R. Katoh, *Ambio* **2012**, *41*, 143.
[110] A. Gürses, M. Açıkyıldız, K. Güneş, M. Sadi Gürses, *Dyes and Pigments*, Switzerland, Springer, US **2016**.
[111] M. Wagstaffe, A. G. Thomas, M. J. Jackman, M. Torres-Molina, K. L. Syres, K. Handrup, *J. Phys. Chem. C* **2016**, *120*, 1693.

SUPPORTING INFORMATION

Additional supporting information may be found online in the Supporting Information section at the end of this article.

How to cite this article: Paredes-Gil K, Páez-Hernández D, Arratia-Pérez R, Mendizábal F. Insights into the role of D-A-π-A type pro-aromatic organic dyes with thieno[3,4-b]pyrazine as A acceptor group into dye-sensitized solar-cells. A TD-DFT/periodic DFT study. *Int J Quantum Chem*. 2020;120:e26108. https://doi.org/10.1002/qua.26108